Universiteit Utrecht

UNIVERSITY COLLEGE UTRECHT

BACHELOR THESIS

The Influence of UV Radiation on the Survival of Meteoritic Organic Compounds

S.A. Luijendijk

supervised by
Dr. Ir. Inge Loes TEN KATE

August 13, 2017

Contents

Part I

Literature Review: Meteoritic Organic Compounds and the Implications on the Development of Life

1. Research thesis

The topic of my research thesis will cover the influence of UV radiation on organic compounds in meteorites. In this literature review I will give an overview of the research that has been done on organics in meteorites and also cover how this relates to the origin of life research field. My research will consist of irradiating Murchison meteorite samples with UV radiation and analyzing their infrared spectra both before and after irradiation. The comparison of the infrared spectra will allow me to identify certain organic compounds in the meteorite and examine whether the UV radiation will cause a change in abundance for these organic compounds.

2. Organic Molecules on Meteorites

Across history meteorites have gotten the attention of civilizations who witnessed their fall. They are impressive enough to have been the subjects of myths and cultish worship. And if we are honest, how can a fiery object falling from the sky not peak your interest. We know now that the sky is not the limit and that these meteorites actually fall to Earth from space. Meteorites are often confused with asteroids or comets, and they are definitely related to each other. The main feature that separates meteorites from asteroids or comets is their location, i.e. a meteorite is simply a piece of some space object that is now on Earth, or another planet or moon, after it survived the journey through the atmosphere and the impact on the surface, whereas an asteroid or comet is a space object that is still in space. If the meteorite is large enough to survive its arrival on Earth, the inside generally remains unaffected by this intense journey. It is this part of the meteorite that provides the extraterrestrial material that is being studied.

2.1. Classification of meteorites

Generally, meteorites are divided into three kinds: stony meteorites, stony-iron meteorites, and iron meteorites. Their names say a lot about their composition. It is mainly the stony meteorites that we are interested in, and they can again be subdivided into chondrites and achondrites, which is derived from their compositional differences (Botta & Bada, 2002). Moreover, chondritic meteorites often contain chondrules, which are round grains or spheroids. These chondrules have a size in the range of millimeters (Whipple, 1966). The chondrites, and especially the carbonaceous chondrites, are considered to be among the most unaltered materials since the solar system formed (Botta & Bada, 2002), and therefore they provide valuable information about the processes that occurred during solar system formation. These carbonaceous chondrites, as their name implies, contain relatively large amounts of carbon in comparison to other chondrites. One of the forms in which this carbon is present in the meteorites is as organic matter, which comprises the largest part of the carbon-bearing compounds in carbonaceous chondrites. Organic matter is often put in the context of life as life deals in organics. And life does leave traces of organics, but traces of organics are not necessarily indicative of life. It is this organic material that is especially interesting, as it provides a record of the existence of organic matter and organic chemical reactions, both predating the origin of life (Sephton, 2014).

The carbonaceous chondrites are again subdivided into, originally, four classes, based on small compositional differences: CI, CM, CO, and CV. Since the original classification, three new classes

have been introduced: CK, CR, and CH. Moreover, there are also unique carbonaceous chondrites that cannot be put in any of these classes (Botta & Bada, 2002).

Then, there is a second manner in which chondrites are classified that indicates their state of alteration and thus how primitive the information in the meteorite is. This classification is called the petrographic type, and it ranges from type 1 to 3 as an indication of the aqueous alteration, with 1 being the most altered and 3 being the least altered, and it also goes on from 4 to 6 for the different stages of thermal metamorphism. As carbonaceous chondrites are among the most primitive meteorites, we have observed no carbonaceous chondrites with petrographic type 4 to 6. So far, only petrographic types 1 and 2 have been observed for carbonaceous chondrites (Botta & Bada, 2002). The Murchison meteorite, for example, is a CM2 meteorite (Hiroi, Pieters, Zolensky, & Lipschutz, 1993).

2.2. Detection of Organic Molecules on Meteorites

The first time the composition of any meteorite was researched was in the 19th century. Wöhler and Hörnes found soluble organic matter when they analyzed the Kaba meteorite in 1859, and organic material was also found in the Orgueil meteorite, that fell in 1864, which they said to be probably of extraterrestrial origin. While the research of meteorite composition was being expanded, the issue of terrestrial contamination became an ever pressing matter. Eventually, in the 1960s, when man journeyed to the Moon, they could compare their results from the meteorites with the well-protected lunar samples. Unfortunately, they were left disappointed, as no amino acids or any important bio-molecules for that matter were detected in these samples (Botta & Bada, 2002). So in order to determine whether the organic compounds found on the meteorites were terrestrial contaminants or indigenous to the meteorites, an ideal sample was required. Such an ideal sample would be free of terrestrial contaminants and be available in relatively large amounts. Moreover, it should contain a wide range of components that are interesting and can be used to test various hypotheses (Sephton, 2014). This ideal sample was obtained in 1969, when a meteorite fell that was observed and quickly sampled, such that little contamination could occur. This was the Murchison meteorite, which provided the opportunity to measure the organic content of a well-protected meteorite with the techniques that had been developed for the lunar samples. Murchison, classified as a CM2, is now among the most extensively analyzed meteorites (Botta & Bada, 2002) and its organic inventory has been used as a general reference to which we can compare other extraterrestrial organic matter (Sephton, 2014). The organic material in meteorites is heterogeneously dispersed in the matrix lithology. This matrix consists of a mixture of high- and low-temperature minerals in disequilibrium. Approximately 30% of the organic material in carbonaceous chondrites consists of soluble organics (Pizzarello & Shock, 2010). The soluble fraction can be characterized by crushing a meteorite sample and treating it with certain solvents of different polarity, which will specifically extract certain compounds of the soluble organic content, such as amino acids or carbohydrates (Botta & Bada, 2002).

Initially, the detection of amino acids in meteorites in the 1960s was discredited and it was attributed to terrestrial contamination. Murchison provided the change to more accurately test for the presence of indigenous amino acids and Kvenvolden et al. (1970) initially found five protein and two non-protein amino acids. The amino acid content of meteorites varies significantly between them, and generally the amino acid content can be correlated with the amount of pre-terrestrial aqueous alteration (Sephton, 2014).

Carboxylic acids are the most abundant solvent extractable compounds in carbonaceous chondrites. In Murchison, carboxylic acids show a complete structural diversity, an equal amount of straight-chain and branched isomers, and a decrease in abundance with an increase in carbon number (Sephton, 2014).

Callahan et al. (2011) looked at the distribution and abundance of nucleobases and their analogs in formic acid extracts of various different kinds of meteorites by Liquid Chromatography Mass Spectrometry (LCMS). They found that 11 out of 12 meteorites that they researched at least contained adenine. Moreover, they found that the Murchison meteorite contains a diverse set of nucleobases, including a few that are very rare on Earth, supporting the theory that they are of extraterrestrial origin.

2.3. Indigenous organic content or terrestrial contaminants

For any measurement of organic content of meteorites it is crucial to determine whether your findings are the results of indigenous organic content of the meteorite or contaminants from Earth. There are various ways to establish this. One way to do this is through isotopic measurements. The stable isotope ratios of hydrogen, carbon, and nitrogen, with heavy isotopes ^{2}H (often denoted as D), ^{13}C, and ^{15}N, have been used extensively to assess the origin of the organic matter (Engel & Macko, 1997). The stable isotope ratio is calculated by comparing the ratio within the sample to ratio of the same compound in an international standard:

$$\delta‰ = \left(\frac{R_{\text{sample}} - R_{\text{standard}}}{R_{\text{standard}}} \right) \times 1000,$$

where R is the ratio between the light and heavy isotope, e.g. ^{2}H/^{1}H (Sephton, 2014).

The organic extracts of meteorites are generally moderately to highly enriched in the heavy isotopes. Terrestrial organic matter, however, with a biogenic origin, is generally depleted in heavy isotopes, as a consequence of biosynthetic processes, such as photosynthesis (Engel & Macko, 1997). The stable isotope ratios for both terrestrial and extraterrestrial organic matter are shown in Figure 1. The reason that organic matter with a biogenic origin is depleted in for instance the heavy carbon isotopes is that photosynthesis causes the isotopic fractionation of carbon with a preference for fixing ^{12}C in plants (Park & Epstein, 1960). This is due to both thermodynamic fractionation as in diffusion, which favors ^{12}C due to its lower mass, and kinetic fractionation through enzymes that have a preference for ^{12}C (O'Leary, 1981).

Another indication of an extraterrestrial origin is the structural diversity of the meteoritic compounds, which would include the presence of compounds that are very rare or even nonexistent in the biosphere (Callahan et al., 2011).

Another way to distinguish terrestrial contaminants from indigenous components, which is only applicable to amino acids, is to look at the chirality of the amino acids (Figure 2). Most amino acids contain an asymmetric center, which allows them to occur in both the laevorotatory (L) or the dextrorotatory (D) form. Generally, the abiotic synthesis of amino acids should result in a racemic mixture, i.e. there is no preference for the L- or D-enantiomer. However, amino acids that are formed by living systems consist exclusively of the L-enantiomer. The choice of either enantiomer

is necessary due to conformational constraints as different molecules are necessary to produce either enantiomer. But why life chose to go with the L-enantiomer rather than the D-enantiomer and whether this was a chance event are still unanswered questions (Engel & Macko, 1997). It is clear, however, that finding a racemic mixture of amino acids is an indication of its extraterrestrial origin.

Despite the general racemicity of amino acids in meteorites, the enantiomeric excess of one or more amino acids has been reported on several occasions. Engel and Nagy (1982) reported the enantiomeric excess of several amino acids, such as alanine and glutamic acid. These results, however, were critized and quickly attributed to terrestrial contaminants. Engel and Nagy (1982) had found non-terrestrial $\delta^{13}C$ values for both L- and D-alanine, indicating their extraterrestrial origin. And later Engel and Macko (1997) further supported their claim by looking at the stable isotope ratio of nitrogen, $\delta^{15}N$, of alanine and glutamic acid, for which they found non-terrestrial values. However, this was not generally accepted as other meteoritic amino acids where influencing the $\delta^{15}N$ value of the researched amino acids, causing the higher value than a terrestrial contaminant would have (Sephton, 2014). After this, more research was done and it was found that some α-methyl-α-amino acids, among which isovaline, show an L-enantiomeric excess. Their extraterrestrial origin was supported by their hydrogen and carbon isotope ratios (Sephton, 2014)

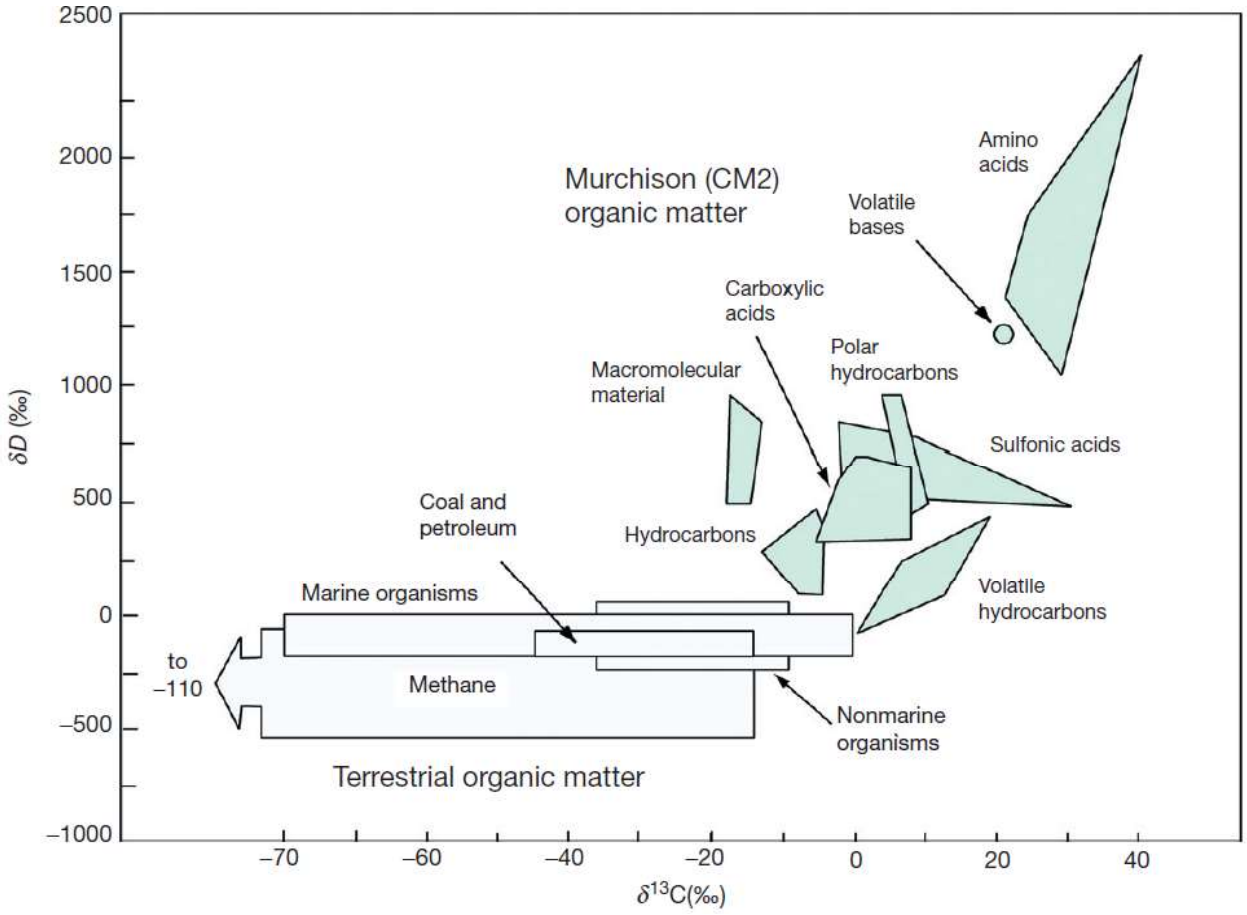

Figure 1: The stable isotope ratios of hydrogen and carbon are shown for terrestrial organic matter (unshaded) and extraterrestrial organic matter (shaded). This illustrates how the two sources provide distinct stable isotope ratios (Sephton, 2014).

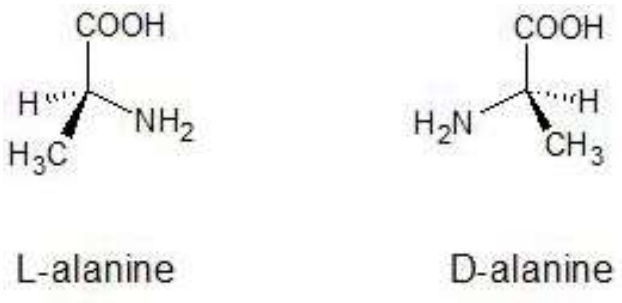

Figure 2: This figure shows the two enantiomers of the amino acid alanine. Enantiomers look quite similar, but they can have very different properties.

as well as the fact that no substantial excesses of L-alanine as other researches had, indicating little terrestrial contamination (Pizzarello & Cronin, 2000).

3. Meteorites and the Origin of Life

Origin of life biology comes with a lot of questions, concerning for example how the first replicatory system arose, when proteins came into play, how did the first cells form, etc. One of the most fundamental of these questions would be how to get from simple abiotic compounds to organic material from which these replicatory systems and proteins are made. Organic compounds are not expected to be readily available on Earth as soon as it was formed. The Universe consists mainly out of hydrogen and helium, and only a small part consists of heavier elements, such as nitrogen, carbon, oxygen, sulphur, and phosphorus, which do occur widespread throughout the Universe (Remusat, 2014). Unfortunately, these elements do not spontaneously form into convenient organic molecules, like amino acids, sugars, or nucleobases, whenever they meet; certain processes are required.

Primordial life on Earth was not nearly as complex as it is right now, and certainly did not require equally complex organic molecules. Nevertheless, we expect some organic molecules to have been present early on. Among these are nucleobases and sugars, so the RNA world can get started, amino acids, so we can move to a protein dominated world, and lipids, for compartmentalization, i.e. cell membranes. Several theories have been put forward on how these organics could have been made available, among which are the abiotic production of organics in hydrothermal vents and the delivery of organics by meteorites.

3.1. The RNA World

One of the leading theories on the origin of life is the RNA world hypothesis. The molecular structure of RNA is shown in Figure 3. The reason we deem RNA to have been so important is that it is both capable of information storage and catalysis. Nowadays, we associate information storage with the rigid molecule that makes up our genes: DNA, and catalysis with the molecules that these genes code for: proteins. But neither can perform the others task; DNA cannot catalyze reactions and proteins cannot store information which can then be copied to form more proteins. A molecule is needed that can perform both, since we cannot expect multiple biopolymers to evolve at the same time while also forming an intricate system of replication, transcription, and translation. This left

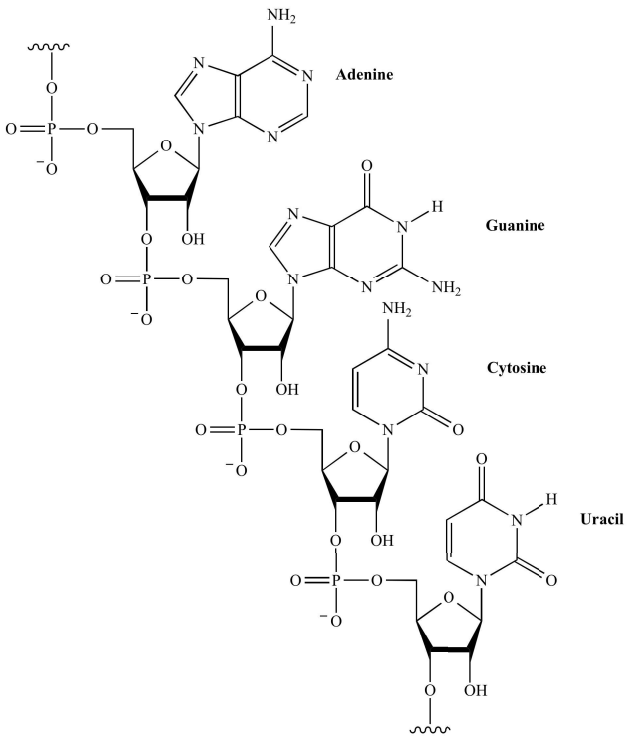

Figure 3: The RNA molecule, consisting of a ribose-phosphate backbone and the four nucleobases uracil, adenine, guanine, and cytosine (Hardinger, n.d.).

us with a “chicken-and-egg" problem. If DNA evolved first, how could it have been replicated or transcribed and translated into proteins if there are no proteins to perform this task? So then proteins must have come first. But proteins are coded for by DNA, and though proteinoids[1] can be formed under specific conditions, they are unstable and have no DNA for natural selection to work on (Neveu, Kim, & Benner, 2013; Rastogi, 2005). That is to say, also for randomly existing proteins, natural selection will favour those proteins with some advantage such as higher stability, but these proteins cannot be replicated and so their advantage is lost. DNA is needed to preserve the advantage some protein might have, e.g. if DNA codes for a protein that stabilizes the DNA itself it will have an advantage and natural selection will favour this DNA. Moreover, if the DNA then mutates such that the protein itself becomes more stable as well, natural selection can again favour this mutation. So a protein can be favourable over others, but natural selection can only work on the DNA coding for the protein.

The solution to this problem is given by RNA. Because it can both store information, as we see in messenger RNA (mRNA), and catalyze reactions, as we see in ribosomal RNA (rRNA), RNA could be capable of self-replication. A self-replication molecule could definitely be subject to natural selection and evolve into bigger and better structures. Then, to move to our modern ribonucleoprotein (RNP) world (Collins, Kurland, Biggs, & Penny, 2009), we require the RNA to gain a peptidyl transferase function, i.e. the ability to bind amino acids and form proteins. And there are convincing indications that RNA would be able to do this. First, in our ribosomes, the protein producing factories of our cells, it is the rRNA that performs the catalytic function of the

[1]Proteinoids are abiotically formed polymers of amino acids. They are generally short and unstable chains.

ribosomes, which was first shown by Noller, Hoffarth, and Zimniak (1992). The proteins of the ribosome probably only provide stability and do not participate in any catalytic activities. Moreover, Zhang and Cech (1997) performed an experiment in which they took an in vitro selection of ribozymes[2] with mainly randomized sequences and selected for peptidyl transferase activity. After a few selection cycles, the experiment did produce RNA sequences with peptidyl transferase activity. However, these sequences were quite specific for the amino acid the experiment was performed with, and could not form peptide bonds between other amino acids as well. Nevertheless, this is still a great support for the RNA world and how it might have evolved into an RNP world.

Based on this theory we can get an overview of the organic molecules we needed to get life started. Ribose, phosphate groups, and nucleobases for the RNA, and amino acids for the proteins. The problem of compartmentalization might not directly have been an issue[3], which will be elaborated on when hydrothermal vents are discussed, but at some points lipids would have been needed to form the first cell membranes.

3.2. The Miller-Urey Experiment

The formation of organics revolves around the fixation of carbon dioxide into organic carbon. The Calvin cycle[4] is currently the most common way of carbon fixation, used by many prokaryotes and all plants. Though the Calvin cycle is the most used pathway for carbon fixation right now, there are still other pathways being used, e.g. the reductive citric acid cycle or the reductive acetyl-coenzyme A pathway (Fuchs, 2011). The first experimentally tested hypothesis that tried to explain the formation of organics through abiotic pathways was given by the famous Miller-Urey experiment from the early 1950s. Their results supported the leading theory on the origin of life at the time, which hypothesized a prebiotic soup in which abiotic compounds would combine to form the building blocks of life (W. Martin, Baross, Kelley, & Russell, 2008). This experiment consisted of two connected flasks representing the ocean-atmosphere system, visible in Figure 4. By shocking the gases present in the flask representing the primitive atmosphere with electrical discharges, representing lightning, energy was added to the system. The idea was that this energy would stimulate reactions between these primordial gases, which would form organic molecules. And indeed, after a few days simple organic compounds were found, including five amino acids (McCollom, 2013).

There are several flaws in this experiment, not the least of which being that the target hypothesis on the origin of life and the hypothesis that this experiment tested are related through highly speculative assumptions (Cleland, 2002). Another critique of this experiment is that it requires an extremely high input of energy for such a small volume, and this is not considered to be realistic as this small volume is representing the entire ocean. Moreover, though through several steps interesting organic compounds such as adenine and guanine were produced, the polymerization of these organic precursors needed a new mechanism to promote their concentration and so this did not happen spontaneously as their formation had (W. Martin et al., 2008).

Since then, many other experiments have been performed and theories have been proposed to

[2]RNA with catalytic activity.

[3]Compartmentalization is needed for the concentration of organics and the control over this concentration. Otherwise, the ocean will just be too dilute for any organic species to properly interact with one another.

[4]In the Calvin cycle the key enzyme RuBisCO is used to fix CO_2 into biomass. The Calvin cycle is also known as the dark reactions, or light-independent reactions, of photosynthesis.

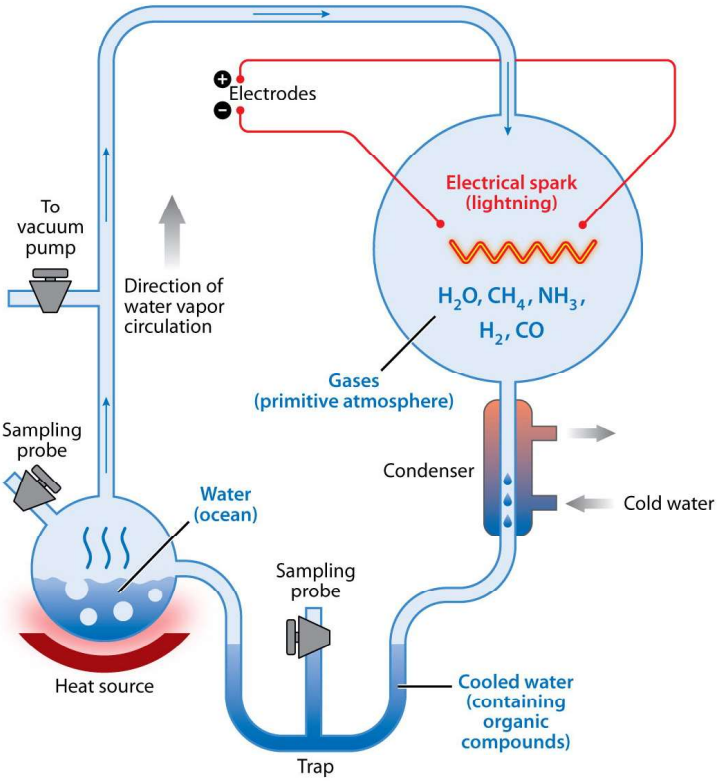

Figure 4: This figure shows the experimental setup of the Miller-Urey experiment. The gases in the atmosphere are subjected to electrical discharges mimicking lightning bolts. This energy is then used to form organic compounds form these simple abiotic compounds (McCollom, 2013).

explain the crucial step towards an Earth on which a reservoir exists with a high enough concentration of prebiotic organic compounds such that it can spark the origin of life. One of the reasons that it is interesting to consider the organic molecules on meteorites, is that these meteorites might have delivered these organic molecules to Earth, contributing to the reservoir of organic compounds. However, one of the theories on the origin of life that has a lot of support revolves around hydrothermal vents.

3.3. Abiotic Production of Organics in Hydrothermal Vents

Hydrothermal vents provide a good solution to the abiotic production of the first organics and there is a considerable amount of arguments supporting these hydrothermal vents to be the location of the origin of life. These vents are globally distributed chimneys around sea-floor spreading zones. Two kinds of hydrothermal vents that are often contrasted are the black smokers and Lost City systems (Kelley, Baross, & Delaney, 2002). Mainly these Lost City systems are interesting for the origin of life, because they are less hot and more stable than black smokers, as they are located tens of kilometers off-axis of the mid ocean ridges they are associated with (W. Martin et al., 2008). Besides that, Lost City systems are alkaline, whereas black smokers are very acidic, which also provides advantages for the origin of life. These Lost City systems are mainly made up out of the magnesium- and iron-rich mineral olivine.

Since the discovery of hydrothermal vents and the chemoautotrophic bacteria and archaea that are living there, the theory that these vents might have been the location of the origin of life has gained support. There are interesting parallels between the metabolic reactions of these prokaryotes that are living there, as well as those of other prokaryotic autotrophs, and the chemistry of the H_2-CO_2 redox couple that is occurring in these hydrothermal vents (W. Martin et al., 2008). The chemistry of life revolves around the reduction of CO_2, so it is not unthinkable to have the first form of life also be dependent on this source of energy, instead of for instance lightning or UV radiation, which no current lifeform uses as its energy source (Sojo, Herschy, Whicher, Camprubí, & Lane, 2016). The reduction of CO_2 with H_2 is performed by acetogens (bacteria) and methanogens (archaea) via the Wood-Ljundahl acetyl-coenzyme A (acetyl-CoA) pathway, and they produce acetate and methane, respectively. Interestingly, this process actually releases energy instead of requiring it, causing them to produce energy and reduce CO_2 at the same time. These favourable thermodynamics and the production of methane or acetate provide the means for producing more complicated biomolecules that can build up a high concentration in these hydrothermal vents (W. Martin et al., 2008). A location where energy can be produced in the same pathway that carbon is fixed, appeared to many as a potential site for the origin of life.

So the questions that remain are: How do we know there was H_2 and CO_2 available in these vents at that time? And how does this reduction yield the energy to produce complex organics? First, the Hadean atmosphere contained much less oxygen and more CO_2 as it was before the dawn of photosynthesis. The CO_2 would have been dissolved in the oceans, also making these oceans more acidic (Sojo et al., 2016). The H_2 required for this process is produced by serpentinization, which occurs naturally as the olivine from the hydrothermal vents comes into contact with ocean water. Serpentinization hydroxylates olivine and in the process releases H_2 and OH^- into the hydrothermal fluids, increasing the H_2 concentration and also making these fluids highly alkaline and reducing (Sojo et al., 2016). Then, methanogens and acetogens use this reduction of CO_2 with H_2 to both synthesize ATP and produce methane and acetate. The process that they use for this is called flavin-based electron bifurcation, which generates highly reactive ferredoxins[5]. The rest of their metabolic pathway is along the aforementioned acetyl-CoA pathway (W. F. Martin, Sousa, & Lane, 2014).

The process of serpentinization also allows for another natural energy source in these hydrothermal vents; a natural ion gradient. The hydrothermal vent effluent is made much more alkaline by the serpentinization process than the surrounding ocean water, making them naturally chemiosmotic (W. F. Martin et al., 2014). Currently, the bulk of energy that is produced in our cells comes from ion gradients, whose energy is tapped through chemiosmotic coupling with the ATPase protein. Needless to say, we cannot expect this protein to have existed before there were even membranes for it to exist in[6]. Hence, it is likely that the phosphorylation of ADP to form ATP through the acetyl-CoA pathway or some variant of it, preceded the use of chemiosmosis (W. F. Martin et al., 2014). However, clearly the hydrothermal vents do provide the path towards chemiosmotic coupling, which is used in all lifeforms today.

[5]Ferredoxins are small FeS proteins.

[6]A membrane is very necessary for chemiosmotic coupling, because an ion gradient cannot be sustained without it; diffusion would quickly get rid of any gradient present. In the hydrothermal vents the gradient exists between the pores and the ocean water, but these “inorganic membranes" could not have contained proteins.

3.4. Delivery of Organic Molecules to Earth by Meteorites

The delivery of organics through meteorites is especially interesting in the context of the Late Heavy Bombardment, which occurred around 700 million years after the formation of the planets and is generally assumed to have ended approximately 3.7 to 3.8 billion years ago (W. F. Bottke et al., 2012; Gomes, Levison, Tsiganis, & Morbidelli, 2005). The earliest evidence of life that is generally accepted within the entire scientific community concerns fossil evidence dated at 3.5 billion years ago (Schopf, Kudryavtsev, Czaja, & Tripathi, 2007). However, micro-fossils have also been found within hydrothermal vent precipitates dating back to at least 3.77 billion years ago (Dodd et al., 2017). Concerning this heavy bombardment, Chyba and Sagan (1992) estimated that the contribution of meteorites during this period was comparable to the organics that were produced by different energy sources, such as UV radiation or impact-shock sources, and they conclude that all could have been a significant factor for the origin of life.

Though it is almost certain that meteorites did bring organic molecules to the prebiotic oceans, the influence and importance of this delivery for the origin and early evolution of life is not clear as of yet. As carbonaceous chondrites contain a broad collection of organics, it is possible that these meteorites brought potential precursors for the origin of life to the Earth (Remusat, 2014). For example, the nucleic acids that have been detected on meteorites and brought to Earth could have been essential for the onset of the RNA world (Callahan et al., 2011). An important question is whether the exogenous delivery of organics to Earth was sufficient enough to make a difference (Kwok, 2011). Supporters of the hydrothermal vent theory might argue that meteorites simply delivered these organics to Earth but that they were not necessary for the origin of life or at the very least that they were not the core cause, as the bulk of the prebiotic organics would have been produced in the hydrothermal vents. Either way, even if meteorites did not contribute in a significant way to the origin of life, they still provide solid proof that the abiotic formation of compounds necessary for life is possible and give insights into how these compounds can be produced abiotically (Pizzarello, 2015).

The amino acids that are often found in carbonaceous chondrites are essential for life on Earth now as they are the building blocks of proteins and enzymes. The detection of amino acids in meteorites supports the extraterrestrial synthesis of biologically relevant compounds. Moreover, the enantiomeric excesses of some amino acids found in meteorites might provide hints as to why current life uses exclusively one enantiomer of the two available ones. Biologically produced amino acids are always L-enantiomers, whereas the abiological synthesis of amino acids generally gives a racemic mixture (Botta & Bada, 2002). On chondrites various enantiomeric excesses have been found for different amino acids, exceeding to a maximum of 18 % (Remusat, 2014). The current singular use of L-enantiomers by life could be a remnant of this enantiomeric excess in the amino acids brought by these meteorites and this would also indicate some contribution to life's origin for the delivery of organics by meteorites (Pizzarello, 2006; Remusat, 2014). Pizzarello (2006) also noted that though the amino acids that show these enantiomeric excesses, such as the 2-methyl-2-amino acids, are not considered important amino acids for our current biochemistry, they might have had a more important role during the onset of molecular evolution. Moreover, 2-methyl-2-amino acids have a strong tendency to form helices following polymerization, which is known to amplify slight initial enantiomeric excesses (Pizzarello, 2006). Hence, this abiotic achirality delivered by meteorites could have pushed life's molecules in the same direction (Pizzarello,

2015).

Another interesting group of non-polar molecules that carbonaceous chondrites contain are able to produce spheres. These sphere producing molecules would have been important in forming the first cell membranes (Remusat, 2014) and have contributed to the self-assembly capabilities of the environment on the early Earth (Pizzarello, 2015). Compartmentalization is incredibly important for life as it for example allows for the concentration of relevant compounds. Moreover, it allows for a differentiation between various compartments based on their reproductive successes (Chyba & Sagan, 1992). Chyba and Sagan (1992) also found that at different pH ranges these non-polar compartments from the carbonaceous chondrite Murchison are able to from two different kinds of boundary structures. At alkaline pH ranges, they form viscous fluid droplets, whereas at acidic pH ranges solid structures are formed. The fact that these non-polar compounds from carbonaceous chondrites could form viscous droplets in alkaline conditions, as are the hydrothermal vents, could still combine well with the hydrothermal vent theory, I think. In the hydrothermal vent theory, life starts out in the micropores of the vents. At some point, when a sufficient energy producing machinery has been established, these “cells" would have left the hydrothermal vents. Now, the micropores cannot provide their compartmentalization any longer, so likely a lipid membrane would have been established for them to be able to leave[7]. The non-polar compounds delivered by meteorites might have been defining in this step. These two mentioned theories therefore do not have to rule each other out.

4. Organic Molecules on Mars

The Late Heavy Bombardment (LHB) was first deduced from the spike in cratering rate observed on the Moon (Gomes et al., 2005; Wetherill, 1975). Various theories on what caused this LHB have been suggested, e.g. the rapid migration of the giant planets or the formation of Neptune and Uranus (W. F. Bottke & Norman, 2017; Gomes et al., 2005; Levison et al., 2001). Regardless of the theory, all are based on the constraints that both the craters on the Moon as well as those on Mars provide, as it is clear that the LHB was an event that all objects in the inner Solar System were subjected to (W. Bottke et al., 2015). As we know that the meteorites that were delivered to the terrestrial planets contained organics, we do expect that Mars received a similar amount of organics as Earth did during that period. Moreover, the current infall of interplanetary dust particles and meteorites on Mars should still deliver organics to Mars with an accretion rate of $\sim 5 \times 10^{-9}\,\mathrm{g\,m^{-2}\,sol^{-1}}$ (Moores & Schuerger, 2012). Because of this currently still present accretion of organics, the Viking landers that were sent to Mars in the 1970s were expected to detect some organics, and it was quite unexpected when they did not (Flynn, 1996). After the non-detection of organics, several processes were suggested that might be responsible for their destruction. Among these processes are the oxidization of organics by some oxidizing source in the soil, glow discharge plasmas created in Martian dust storms that can produce reactive species, and degradation of organics by UV radiation (ten Kate, 2010). More recently, the Sample Anal-

[7]An interesting side note on membranes: there are fundamental differences between the phospholipids of the membranes of archaea and bacteria. Namely, archaeal phospholipids are linked through ether bonds, whereas those of bacteria are linked through ester bonds (Sojo, Pomiankowski, & Lane, 2014). This indicates that the divergence between bacteria and archaea occurred before they left the hydrothermal vents, before they needed the proper membranes to live in the open ocean. So then the Last Universal Common Ancestor (LUCA), the very last point before the tree of life started to grow branches, must have lived in these hydrothermal vents.

ysis at Mars (SAM) experiment, which generally has a higher diagnostic power than the Viking anders did (Mahaffy et al., 2012), has detected organics in the Martian soil (Millan et al., 2017). Especially in light of these findings and the fact that water likely existed on Mars during its early history (Carr, 1987) as well as the organics that must have been delivered during the LHB, it is interesting to ask why life does exist on Earth but not on Mars (anymore). Models of hydrothermal systems have even been suggested for Mars (Varnes, Jakosky, & McCollom, 2003). The influence of UV radiation can be an interesting aspect to look at when considering life on Mars. Life on Earth and organic compounds likely were protected from UV radiation by the oceans they resided in for a long time, until a substantial ozone layer was built up after the invention of photosynthesis, whereas the ocean on Mars could have dried up before any substantial protection layer could have been formed, resulting in the sterilization of the planet.

Part II

Research Thesis: The Influence of UV Radiation on the Survival of Meteoritic Organic Compounds

The Influence of UV Radiation on the Survival of Meteoritic Organic Compounds

S.A. Luijendijk

August 13, 2017

Abstract

UV radiation is known to be destructive for organic compounds and it could of great influence origin and evolution of life in worlds where there is little to no protection from this UV radiation. Life on Earth likely was only able to venture to more superficial areas of the ocean after a substantial ozone layer was established. UV radiation is probably also causing the destruction of organic compounds, delivered by meteorites and interplanetary dust particles, in the top layer of the soil on Mars. Because meteoritic delivery is one of the main and sure ways through which organics can reach a planet, the influence of UV radiation on these compounds is important in the origin and evolution of life context. In this research, a method is employed in which a sample with Murchison meteorite is irradiated and analyzed using Fourier Transform Infrared Spectroscopy (FTIR). The infrared spectra that were obtained show a general decrease in organic content. In particular, the change in hydrocarbon, carboxylic acid, and amino acid content was examined. This method is a good way to get a first look at the effects of UV radiation for your sample and can help in identifying what your next step should be. However, it was found that due to the complexity of the infrared spectra this method cannot provide any in depth quantitative or qualitative analysis of the effects of UV radiation.

1. Introduction

In the origin of life field there are various theories on how the first organic molecules became available on Earth. Namely, it is not obvious that these organic molecules and precursors to life would have been readily available on an early Earth. Various processes have been suggested, among which are a reductive acetyl-coenzyme pathway, energy-driven reduction of ferredoxin, or a reductive citric acid cycle (Fuchs, 2011). Another way that might have contributed to the overall organic content on Earth is extraterrestrial delivery through meteorites or interplanetary dust particles (IDPs). The possible contribution of meteorites and IDPs was evaluated by Chyba and Sagan (1992) as well as compared to the production of endogenous sources considered at that time. An important difference between the early Earth and the current Earth is that the former did not have an ozone layer protecting the life on it from the destructive UV radiation coming from the Sun. These organic molecules could have been affected by UV radiation through for instance photolysis. Though no ozone layer was available at that time to protect the organics, the ocean could have possibly performed this protection task and so a reservoir of organics could build up.

Samples				
	1	2	3	4
Exposure time (h)	96	48	72	96
UVA (W/m^2)	420.5	188.7	38.7	33.5
UVB (W/m^2)	48.0	17.9	5.4	4.5

Table 1: This table shows the exposure times and intensities of the pre-irradiated Murchison samples (Chrysostomou, 2014).

When we look at Mars currently, we see that it does not have an ozone layer, or any atmosphere really. Besides that, no ocean is currently available there to protect organics from the UV radiation that reaches Mars. So any organics that are delivered to the Martian surface by meteorites or IDPs are very much exposed to the destructive forces of UV radiation (ten Kate, 2010). With this research I aim to characterize the influence of UV radiation on organic molecules in meteorites. For this research I received a piece of the Murchison meteorite, which fell in 1969 in Murchison, Australia. This is a carbonaceous chondrite with a high organic content. Murchison was collected very quickly after it fell, minimizing the amount of terrestrial contamination. Upon initial analysis it was found that it was indeed in pristine condition. Its condition and the large mass and thus high availability, make it one of the most studied meteorites (Botta & Bada, 2002). The Murchison sample used in this study was exposed to various intensities of UV radiation for various times and hereafter it was analyzed using Diffuse Reflectance Infrared Fourier Transform Spectroscopy (DRIFTS).

2. Materials and Method

All the Murchison samples that was used for this research I received from Seraina Holinger. In the first part of my research I used samples that were already irradiated upon receiving them with the intensities and times according to Table 1. Hereafter, I received some pure Murchison which I irradiated myself. The pre-irradiated samples were analyzed using DRIFTS, which is a kind of Fourier Transform Infrared Spectroscopy (FTIR). The four Murchison samples were mixed with KBr. For samples M1, M3, and M4, the mixture consisted of approximately 10 wt% Murchison and 90 wt% KBr. However, for sample M2 there was not enough of the sample available to have 10 wt% of Murchison and still fill up the sample cup. As 10 wt% is advised to be an upper limit of your amount of sample when using DRIFTS (Bradley, n.d.), using a lower relative amount of Murchison should not create any issues. So for sample M2, 5 wt% Murchison was mixed with 95 wt% KBr.

To measure the spectra, I used the ThermoFisher FTIR and the OMNIC Specta Software. Before measuring the spectra of the Murchison samples, a background spectrum was measured of a sample cup filled with pure KBr. Before each Murchison sample measurement, there is a 2 minute N_2 flush of the chamber to reduce interference from atmospheric gases.

For the part of the research where we irradiated the samples ourselves, a piece of 0.2030 g of Murchison was ground using a pestle and mortar. Before irradiating this sample, an IR spectrum was taken of the non-irradiated Murchison with the FTIR. Approximately 5 wt% Murchison was

Pre-irradiated samples				
	M1	**M2**	**M3**	**M4**
Rel. amount of Murchison (wt %)	10.9	5.5	10.7	10.5
Mass in FTIR (g)	UNK	UNK	0.0185	0.0240

Table 2: This table shows the relative amounts of Murchison in the Murchison KBr mixtures that were prepared for the FTIR measurements of the samples that were irradiated by Kyriacos Chrysostomou as well as the masses of the samples that were placed in the FTIR. The masses the samples in the sample cups for M1 and M2 are unknown as they were forgotten to be measured.

Our irradiated samples							
	NI	**UV1**	**UV2**	**UV3**	**UV4**	**UV5**	**UV6**
Mass in UV chamber (g)	N/A	0.0066	0.0069	0.0274	0.0227	0.0096	0.0085
Rel. amount of Murchison (wt %)	5.3	5.3	5.7	5.3	5.3	5.3	5.4
Mass in FTIR (g)	0.0212	0.0205	0.0242	0.0274	0.0227	0.0239	0.0205

Table 3: This table shows the masses of the samples UV1-UV6 when they were placed inside the UV chamber. It also shows the relative amounts of Murchison in the Murchison KBr mixtures that were prepared for the FTIR measurements for the non-irradiated (NI) sample as well as the samples UV1-UV6. The masses of the samples that were placed in the FTIR are also shown. Notably, as UV3 and UV4 were already mixed with KBr upon entering the UV chamber, their masses were the same in the UV chamber as in the FTIR.

mixed with 95 wt% KBr.

A total of six sample cups were placed inside the UV irradiation chamber. Samples UV1 and UV2 contained a thin layer of pure Murchison. Samples UV3 and UV4 were filled up with a 5 wt% Murchison 95 wt% KBr mixture. It was decided to do this because the UV lamp would mainly affect the top layer of the samples in the sample cups. If UV1 and UV2 would then be mixed with KBr to analyze their spectra, the effects of the UV radiation might decrease due to the mixing. Namely, even though for DRIFTS the radiation passes through the entire sample and builds up the infrared absorptions and reflections, the top layer still contributes most to the spectrum. To see if this might be an issue, samples UV3 and UV4 were added. By directly radiating the Murchison KBr mixtures in UV3 and UV4, the samples can immediately be entered into the FTIR after irradiation without having to mix the sample and possibly redistributing the irradiation effects. Samples UV5 and UV6 contained a thin layer of pure Murchison and a drop of distilled water to see what the effects of a small amount of H_2O might be on the UV interaction with the sample.

Then, samples UV1, UV3, and UV5 were placed underneath the UV lamp in the radiation chamber, whereas UV2, UV4, and UV6 were placed next to them and were separated from the other samples by a metal plate. Before the UV lamp was turned on a mass spectrum was taken of the gases inside the instrument. After 22 h two more mass spectra were taken. One of the gases inside the instrument, and one were a small amount of the gases from the chamber were released to the mass spectrometer to see what gases had built up inside the UV chamber. The temperature inside the chamber was set at 20 °C and the pressure in the chamber was set to near vacuum at approximately 10^{-6} mbar. The intensity of the UV lamp was set at approximately 375 W/m^2.

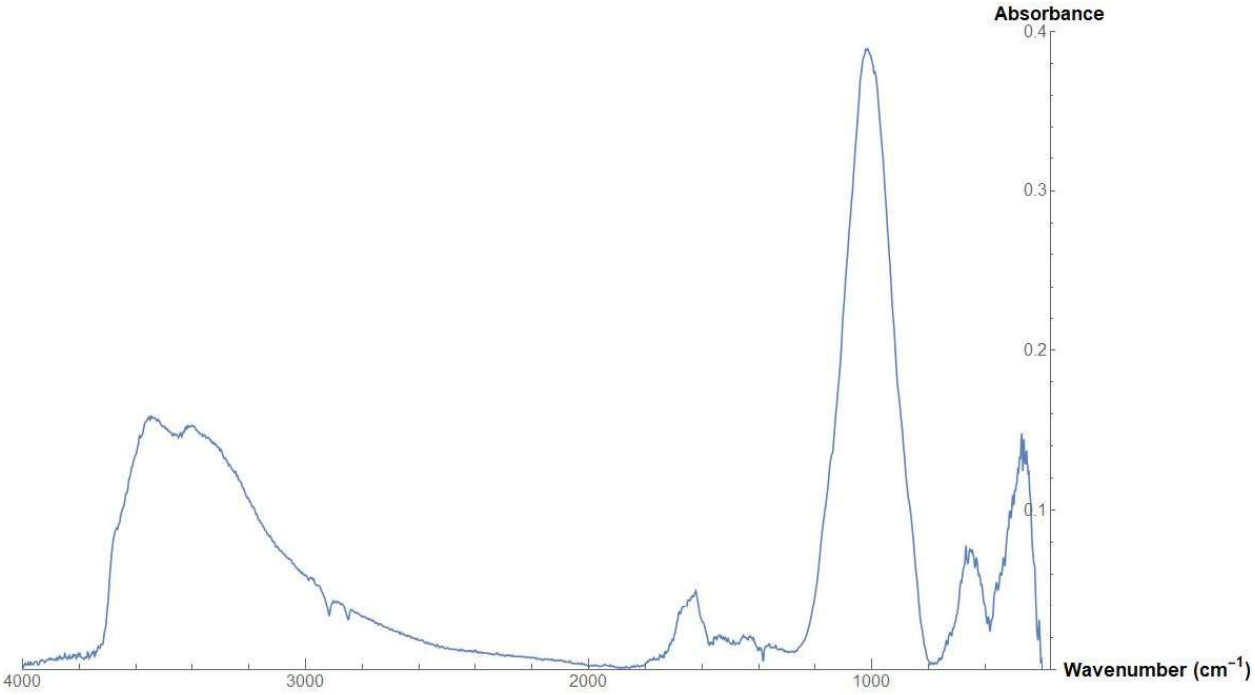

Figure 1: In this figure the complete baseline-corrected IR spectrum that followed from the FTIR measurements of the NI sample is shown. The NI spectrum without baseline correction is given in Figure S1.

After 24 h the lamp and pressure pump were turned off and the valves were opened to allow the pressure in the chamber to equilibrate to atmospheric pressure. After the pressure inside the chamber had reached atmospheric levels, the samples were taken out and prepared for FTIR analysis. Samples UV3 and UV4 were analyzed immediately with the FTIR. Samples UV1, UV2, UV5, and UV6 were mixed with KBr in an approximate 5 wt% Murchison 95 wt% KBr ratio. Then, their spectra were also measured in the FTIR. A complete overview of the exact masses and KBr ratios for the different samples is given in Tables 2 and 3.

3. Results

3.1. Non-irradiated Murchison

The baseline-corrected IR spectrum that followed from the FTIR analysis of the non-irradiated (NI) Murchison sample mixed with KBr is shown in Figure 1.

3.1.1. Mineral composition

One of the most defining features in these IR spectra is the peak around 1000 cm^{-1}, which represents the Si−O stretching vibrations and provides information on the mineral composition of the sample, shown in Figure 2. This region is generally a quite complicated one, but can give a lot of information on the mineral species as every mineral produces a different pattern (Chukanov, 2013). Within the mineral matrix previous studies have found examples of clay minerals, olivines, troilites, magnetites, and several serpentines (Beck et al., 2014; Sephton, 2013). Minerals from the

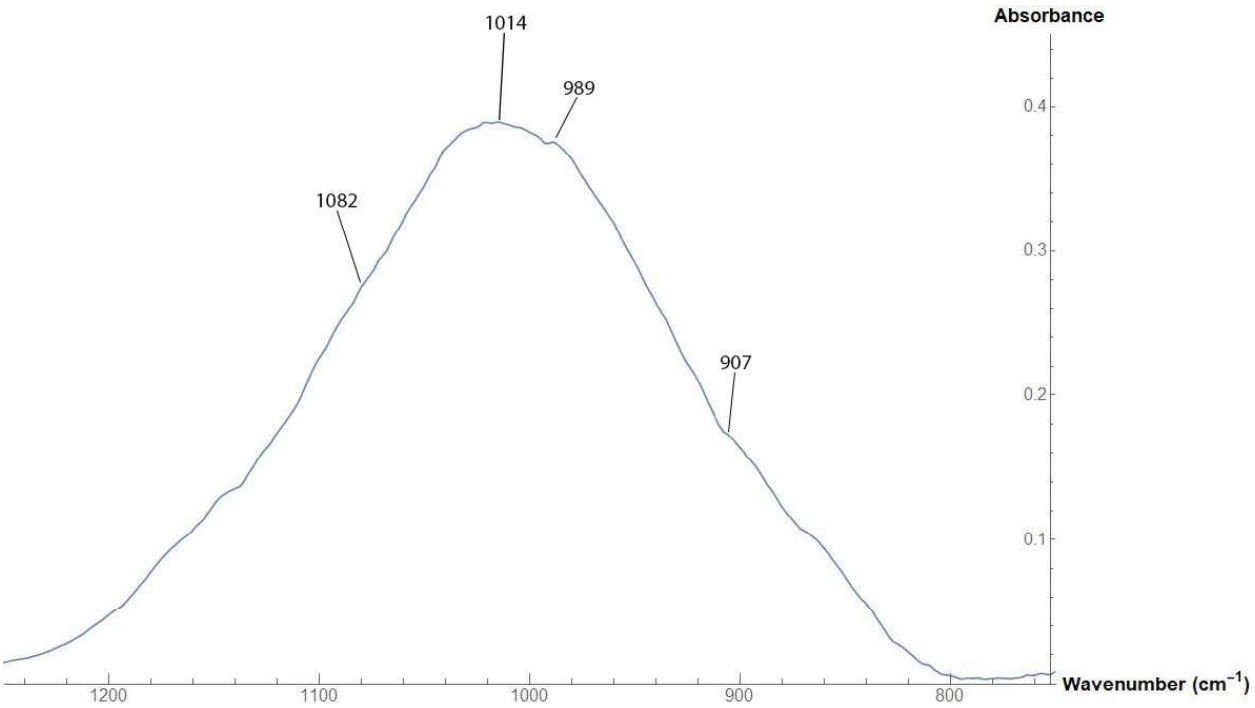

Figure 2: In this figure the baseline-corrected IR spectra of the 1000 cm^{-1} region with indicated peaks of the NI sample is shown.

serpentine group, in general a mixture between a Mg-rich serpentine (such as chrysotile, lizardite, and antigorite) and Fe-rich cronstedtite, are generally found to be the dominant phase (Beck et al., 2014). Beck et al. (2010) concluded that the central peak around 1000 cm^{-1}, representing the phyllosilicate phases, has no comparison with any commonly observed terrestrial serpentine spectra and that they appear to be spectroscopically distinct from any terrestrial phyllosilicates. The silicate absorption band measured is broad and symmetric, which does not agree with any terrestrial phyllosilicates (Beck et al., 2014). It is likely that this region is built up of a complex mix of highly disordered serpentine minerals. Beck et al. (2014) attempted to linearly combine the spectra of several terrestrial phyllosilicates (saponite, lizardite, antigorite, chrysotile, and cronstedtite), but no combination could reproduce the measured Murchison spectrum in the 1000 cm^{-1} region. Moreover, the spectra of these terrestrial phyllosilicates do not correspond to the Murchison spectrum in the 3 μm region (Beck et al., 2010). Beck et al. (2010) concluded that it should not be preferred to say that the Murchison matrix is mainly cronstedtite, but instead they advise to use the term Fe-rich serpentine.

Looking at the spectrum in Figure 2, there are indications of the presence of several serpentines such as cronstedtite, which has a strong peak around 902 cm^{-1}, and antigorite, which has strong peaks around 1082 and 987 cm^{-1} (Chukanov, 2013). However, the broad symmetric peak we observe more resembles saponite, which has a strong peak around 1015 cm^{-1}. Moreover, as Beck et al. (2010) also noted, the spectra of these minerals do not correspond with our measured spectrum in the 4000-3000 cm^{-1} region. An explanation given by Beck et al. (2014) for the unexpected saponite-like features observed in the 1000 cm^{-1} region is the substitutions of cations in the serpentines. Coupled substitutions of Al – Si and Mg – Al can induce a broadening of the Si – O

feature, and the serpentines of CM2 meteorites such as Murchison are likely to be highly substituted by Al^{3+} and Fe^{3+}, which could produce these saponite-like features. Besides that, despite of the difference between the spectra of Murchison and terrestrial serpentines, there is still sufficient indication of their presence (Barber, 1981).

3.1.2. Hydrocarbons

Murchison contains 12-35 ppm aliphatic hydrocarbons and 15-28 ppm aromatic hydrocarbons (Sephton, 2013). Cronin and Pizzarello (1990) found that the primary aliphatic hydrocarbons in Murchison are a diverse group of branched, alkyl-substituted, mono-, di-, and tricyclic C_{15} to C_{30} alkanes. The high branching of these alkanes can be seen from the methyl and methylene absorption bands in the 3000-2800 cm^{-1} region. A roughly equal strength of the methyl and methylene absorption bands indicates a relatively high amount of methyl groups and thus branchedness of the alkanes (Cronin & Pizzarello, 1990). In Figure 3a this region is amplified. However, due to two dips in our spectrum caused by a difference in atmosphere from the KBr background spectrum and the spectrum measured for the Murchison-KBr sample, the methyl and methylene absorption bands are poorly visible. Especially, the methylene bands are supposed to be at the exact place where the dips occur in the measured infrared (IR) spectrum. Moreover, the peaks occur in a region where the spectrum has a slope, so to improve the visibility a line was fitted to the 3100-2700 cm^{-1} region and subtracted from the spectrum, the result of which is shown in Figure 3b. The methyl peaks are now better visible around 2870 and 2960 cm^{-1}, though there is some noise in the spectrum.

3.1.3. Carboxylic acids

Murchison contains approximately 332 ppm monocarboxylic acids. Murchison contains an equal amount of branched and straight chain isomers. Also, there is a general decrease in amount with an increase in carbon number. In total, over 50 different monocarboxylic acids have been detected, with propanoic acid being the most abundant one (Sephton, 2013). C=O bonds generally show an absorption band in the $1760 - 1675\,cm^{-1}$ region and specifically there is a strong C=O stretching band of acids around $1700\,cm^{-1}$ (Martin & Gilbert, 2011). In Figure 4a this region of the spectrum is shown, in which some peaks can be seen, though some might be due to noise. In particular, the peak at $1682\,cm^{-1}$ can represent the absorption through the C=O stretching vibration. Besides that, a broad band in the $3000 - 2600\,cm^{-1}$ region, shown in Figure 4b, superimposed on the peaks due to C−H stretching is a strong indicator of carboxylic acids (Martin & Gilbert, 2011). However, there is not a clear broad band visible in this region, but it might also be hidden by other absorptions as there is some general absorption in that region forming a slope.

3.1.4. Amino acids

Murchison contains approximately 60 ppm amino acids. These indigenous amino acids consist of both protein and non-protein amino acids. Moreover, they exist as racemic mixtures and show structural diversity. Even the amino acid isovaline, which cannot undergo secondary racemization, was found as a racemic mixture in Murchison (Lawless, 1973). This finding gives a strong indication of the production of amino acids as a racemic mixture, meaning their origin is non-biological. Over 80 amino acids have been detected on Murchison, most of which seem to be unique to carbonaceous chondrites (Sephton, 2013). The amino acids that have been identified in Murchison

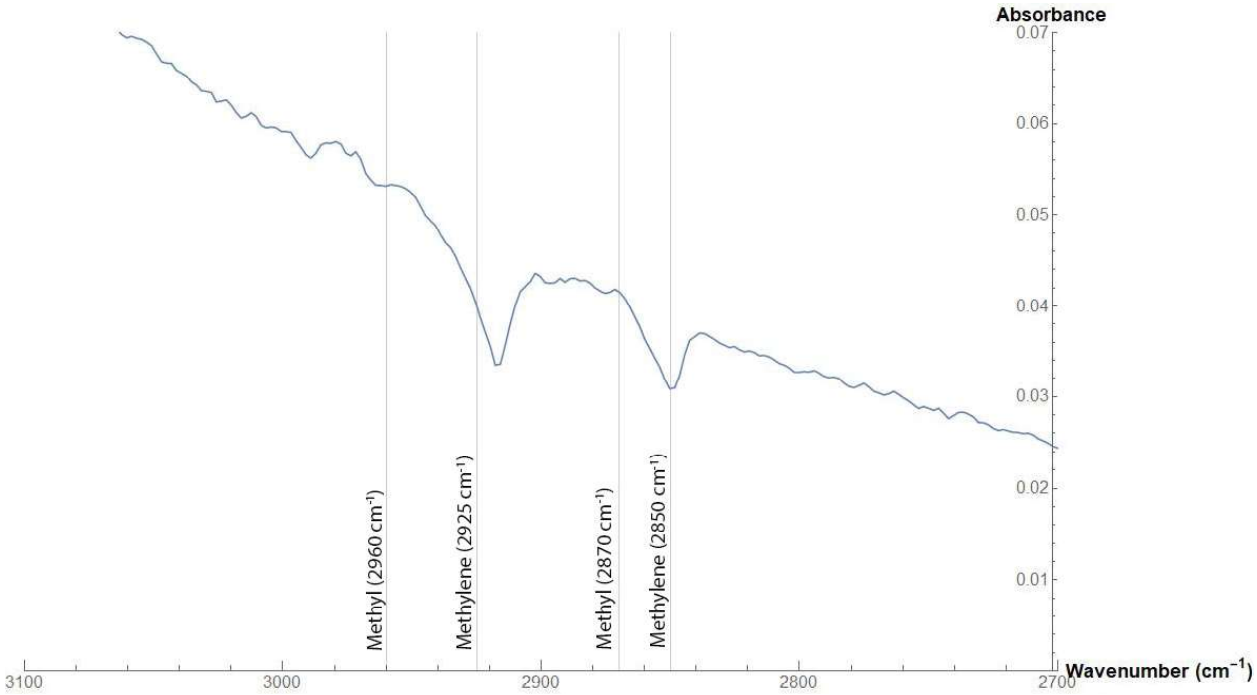

(a) This figure shows where the absorption peaks for methyl and methylene groups should be located in the $3000 - 2800\,\mathrm{cm}^{-1}$ region.

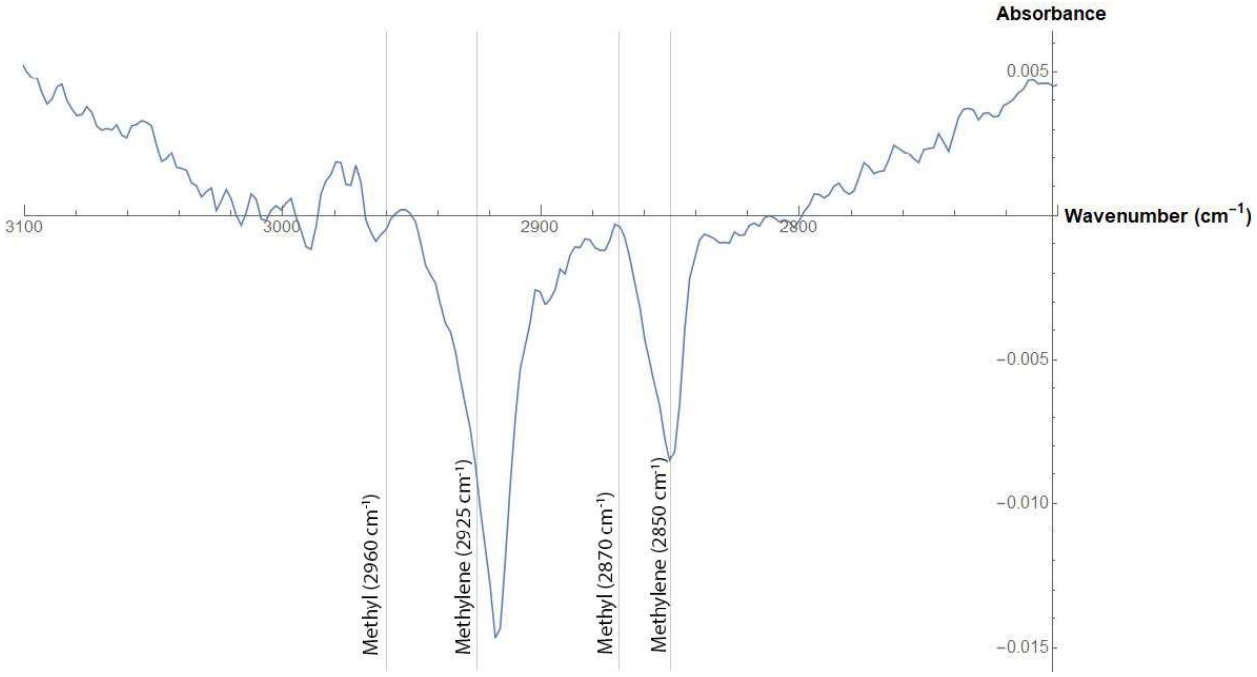

(b) This figure shows the deviation of the data from a line fitted to the spectrum in the $3100 - 2700\ \mathrm{cm}^{-1}$ region and the locations where we expect to find the methyl and methylene peaks.

Figure 3

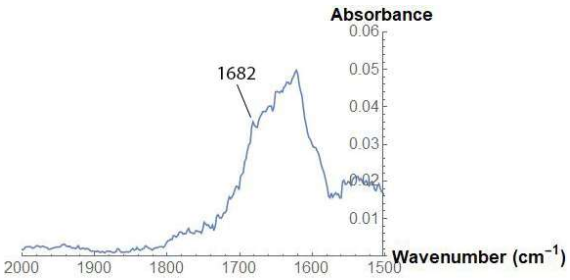

(a) This figure shows the C=O stretching peak at 1682 cm^{-1}.

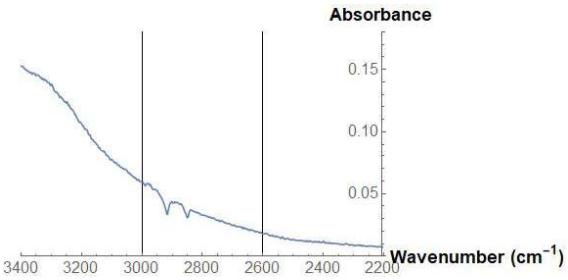

(b) This figure shows the $3000-2600\,\mathrm{cm}^{-1}$ region, which should show a OH band to indicate carboxylic acids.

Figure 4

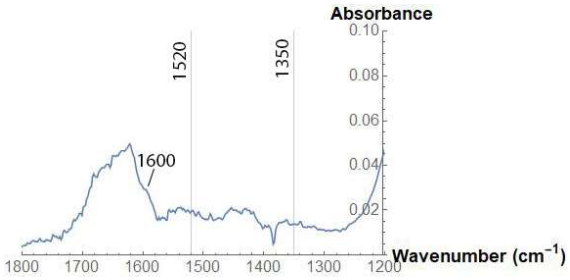

(a) This figure shows the NH_2 bending peak at 1600 cm^{-1} and where the 1520 and 1350 cm^{-1} NH_2 coupled stretching bands are expected to be.

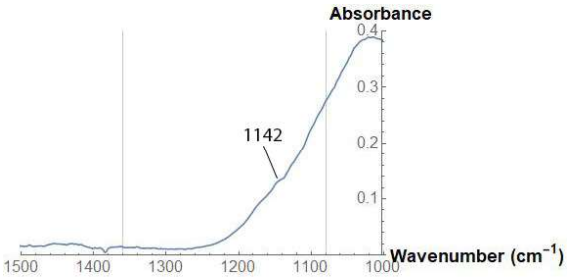

(b) This figure shows the region in which we expect to find a band due to the C–N stretching vibration. The peak at 1142 cm^{-1} might be due to this vibration.

Figure 5

include more unusual amino acids, such as isovaline and pseudoleucine, as well as more common amino acids to Earth, such as glycine, alanine, and glutamic acid (Engel & Nagy, 1982).

One of the bands often used to characterize primary amines is the NH_2 bending band at 1600 cm^{-1} (Martin & Gilbert, 2011) and this band can indeed be identified, as shown in Figure 5a. However, two other bands, associated with an NH_2 coupled stretching vibration at 1520 and 1350 cm^{-1}, which should be a pair of intense bands, are not clearly visible at all. A small peak can be seen at the 1350 cm^{-1} location, but it is not clear if this is noise or a peak. Besides that, a C–N stretching band should occur between 1360 and 1080 cm^{-1} (Martin & Gilbert, 2011), and so the peak at 1142 cm^{-1} could be attributed to this C–N stretching vibration (Figure 5b).

3.2. Our irradiated samples

The results from the FTIR measurements of our irradiated samples, i.e. UV1-UV6, are combined with the NI Murchison spectrum in Figure 6. In the following section some interesting differences between the spectra concerning several organic compounds will be highlighted.

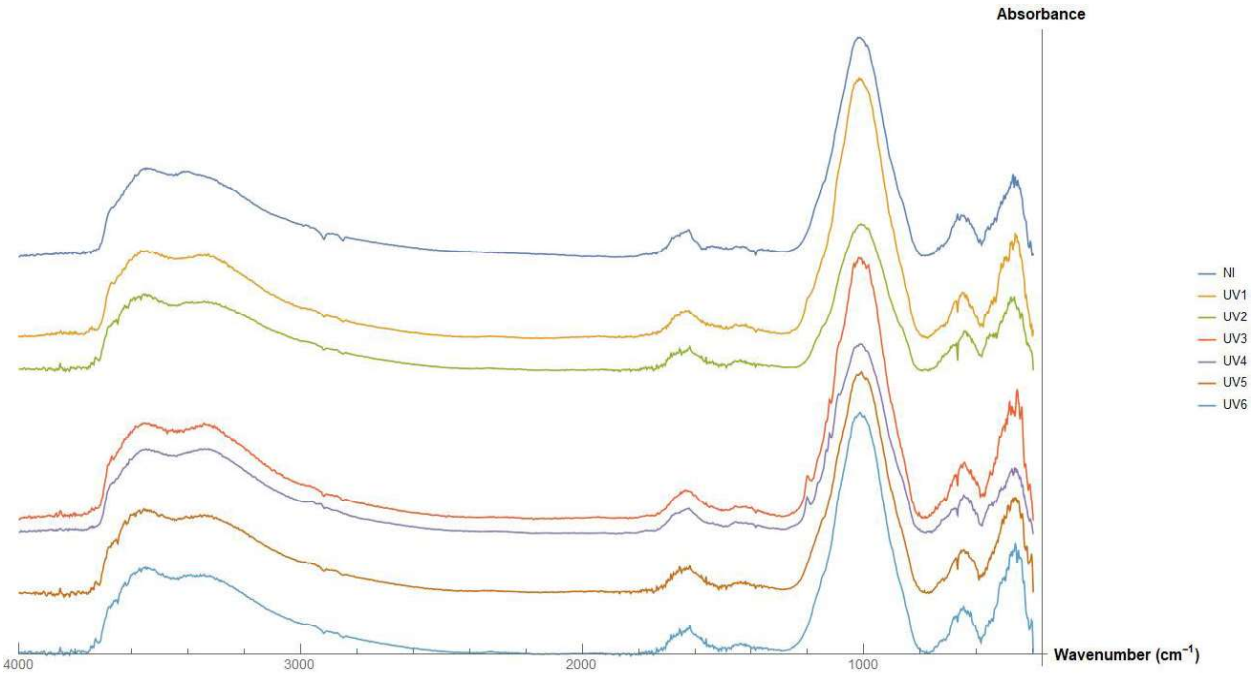

Figure 6: In this figure the complete baseline-corrected IR spectra that followed from the FTIR measurements of samples UV1-UV6 are stacked on top of each other together with the NI spectrum. The absolute absorbance is therefore not given. The seven spectra are given with their absolute absorbance without baseline correction in Figure S2 and with baseline correction in Figure S3.

3.2.1. Hydrocarbons

The UV1 and UV2 samples, shown in Figure 7a, both show the methyl absorption bands at 2960 and 2870 cm^{-1}. In fact, for the 2960 cm^{-1} it is even better visible in these two samples than in the spectra of the NI sample. Interestingly, the UV2 spectrum also shows a slight peak at 2925 cm^{-1}, which indicates the presence of methylene groups. Concerning the methylene band at 2850 cm^{-1}, UV1 and UV2 both also show a dip, related to the background spectrum, similar to the NI spectrum. However, at a slightly higher wavenumber both UV1 and UV2 have a small peak, at approximately 2854 cm^{-1}.

Figure 7b shows the UV3 and UV4 spectra compared to the NI spectrum. UV4 shows really clear methyl and methylene peaks at 2960 and 2925 cm^{-1}. The UV4 spectrum also shows a small peak at a slightly higher wavenumber for the 2850 cm^{-1} methylene peak. The methyl peak at 2870 cm^{-1}, however, is not as apparent as the other ones. The UV3 spectrum also shows a peak region for the methyl 2960 and 2870 cm^{-1} bands. The spectrum also shows a slight peak for the 2925 cm^{-1} methylene band, but nothing can be seen for the 2850 cm^{-1} band.

Figure 7c shows the UV5 and UV6 spectra compared to the NI spectrum. Both UV5 and UV6 show the methyl 2960 and 2870 cm^{-1} peaks, but the 2870 cm^{-1} seems to be either quite a bit weaker for UV5 or shifted towards a higher wavenumber. UV5 does not show any methylene bands, whereas UV6 does show a slight peak at the 2925 cm^{-1} methylene band. Moreover, it also shows a slight peak to the left of the 2850 cm^{-1} band, also at 2854 cm^{-1} just like the UV1, UV2, and UV4 spectra, indicative of methylene groups.

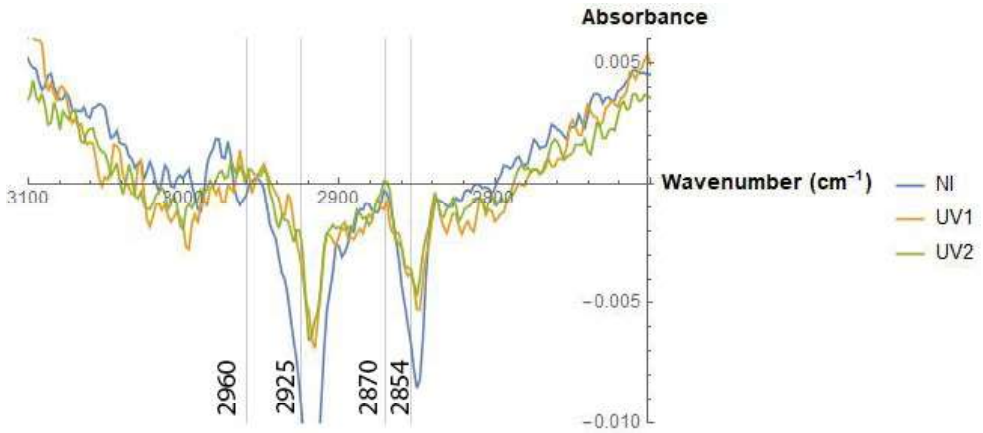

(a) This figure shows the methyl and methylene absorption peaks for the NI, UV1, and UV2 samples. Similar to Figure 3b, this figure was produced by fitting a line to the $3100 - 2700\,\mathrm{cm}^{-1}$ region and subtracting it from the spectrum.

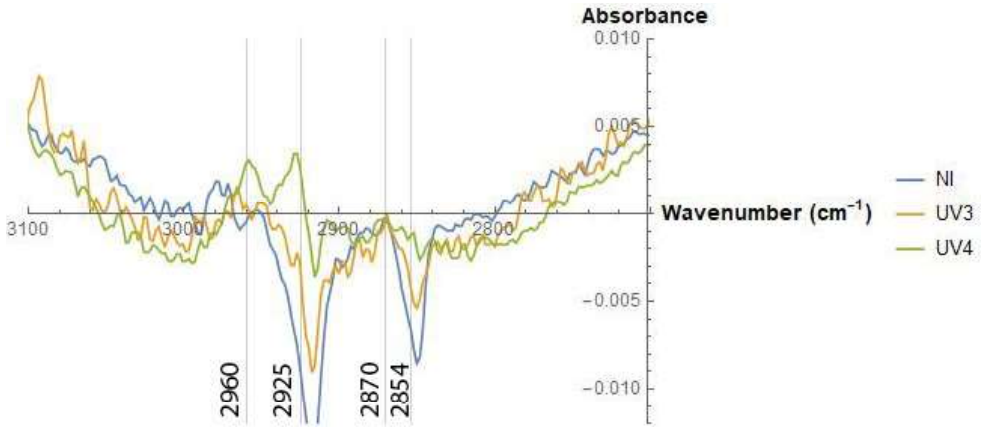

(b) This figure shows the methyl and methylene absorption peaks for the NI, UV3, and UV4 samples. Similar to Figure 3b, this figure was produced by fitting a line to the $3100 - 2700\,\mathrm{cm}^{-1}$ region and subtracting it from the spectrum.

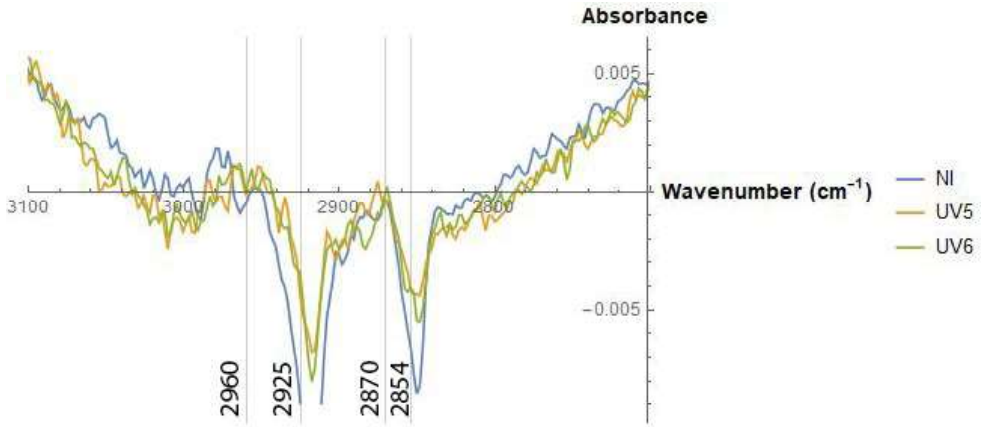

(c) This figure shows the methyl and methylene absorption peaks for the NI, UV5, and UV6 samples. Similar to Figure 3b, this figure was produced by fitting a line to the $3100 - 2700\,\mathrm{cm}^{-1}$ region and subtracting it from the spectrum.

Figure 7

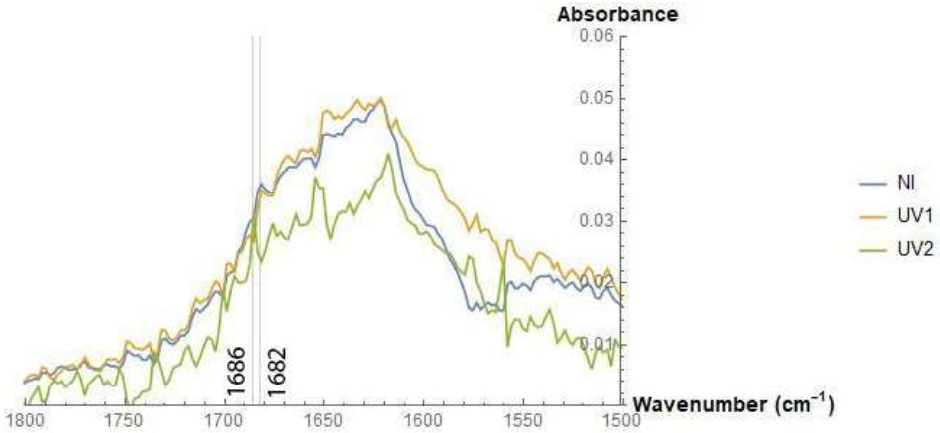

Figure 8: This figure shows the C=O absorption region of the UV1 and UV2 spectra, and the NI spectrum. In particular, the peaks at approximately 1686 and 1682 cm^{-1} might be due to the C=O stretching absorption.

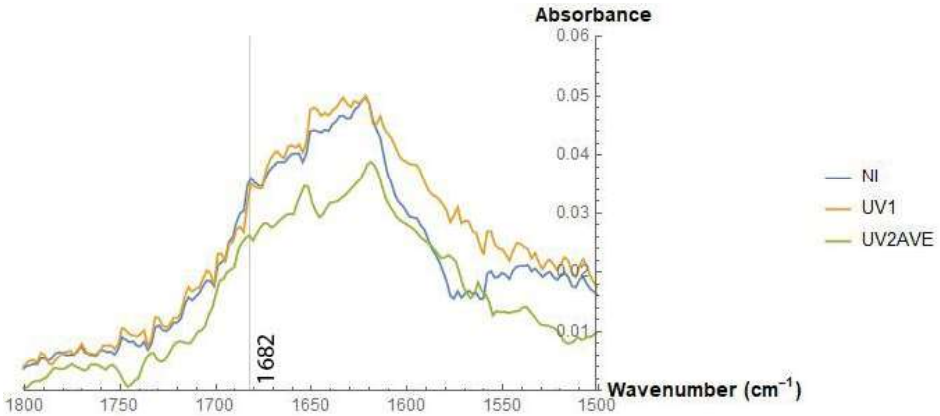

Figure 9: This figure shows the C=O absorption region of the UV1 and averaged UV2 spectra, and the NI spectrum. In particular, the peaks at approximately 1682 cm^{-1} might be due to the C=O stretching absorption.

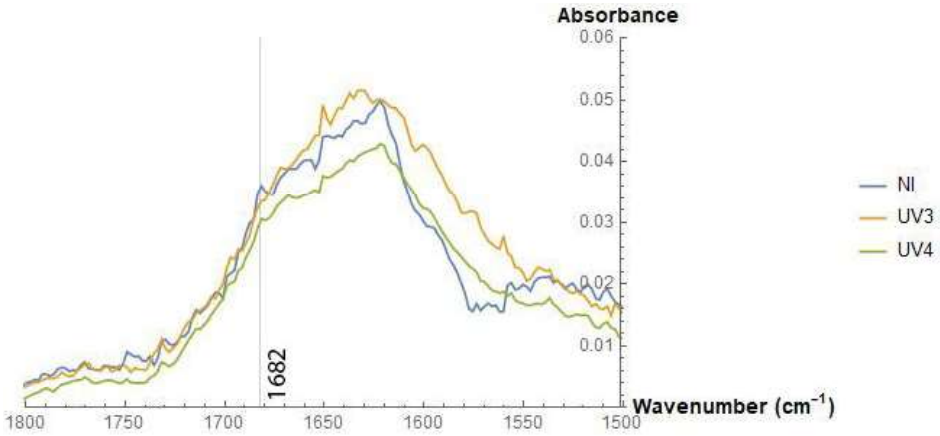

Figure 10: This figure shows the C=O absorption region of the UV3, UV4, and NI spectra. In particular, the peaks at approximately 1682 cm^{-1} might be due to the C=O stretching absorption.

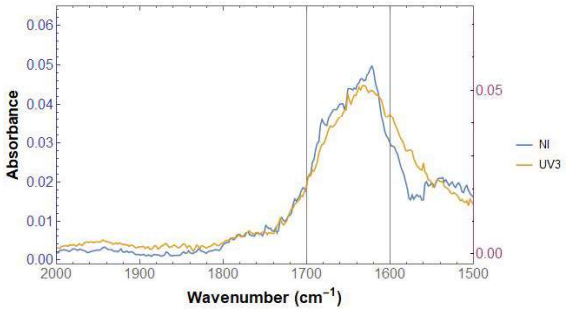

(a) This figure shows the C=O absorption region of the UV3 and NI spectra. In particular, it shows how the UV3 spectrum is roughly the same as the NI spectrum, except for the $1700-1600\,\mathrm{cm}^{-1}$ region, where it shows a relatively lower absorbance.

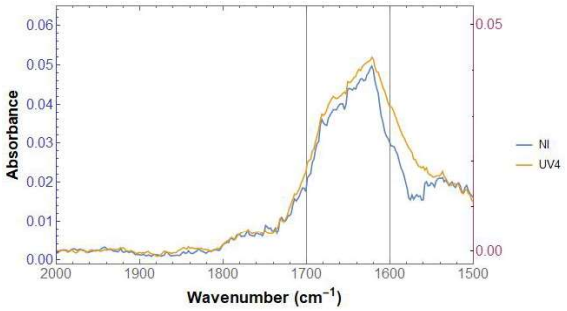

(b) This figure shows the C=O absorption region of the UV4 and NI spectra. In particular, it shows how the UV4 spectrum is roughly the same as the NI spectrum, except for the $1700-1600\,\mathrm{cm}^{-1}$ region, where it shows a relatively higher absorbance.

Figure 11

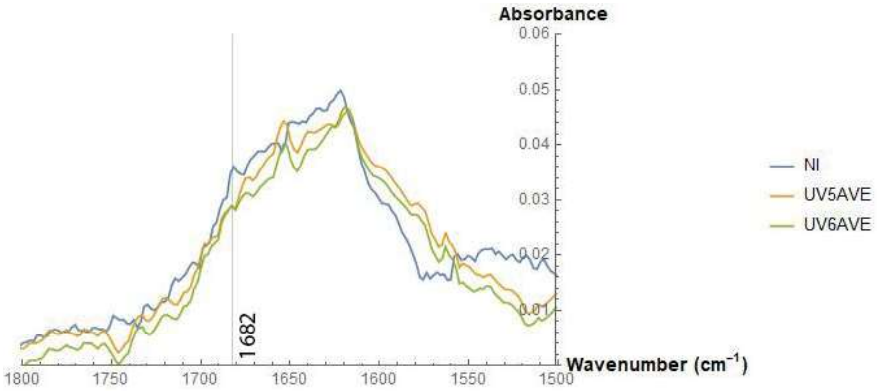

Figure 12: This figure shows the C=O absorption region of the averaged UV5 and UV6 spectra, and the NI spectrum. In particular, the peaks at approximately $1682\,\mathrm{cm}^{-1}$ might be due to the C=O stretching absorption. The non-averaged spectra for this region are shown in Figure S4.

3.2.2. Carboxylic acids

As can be seen in Figure 8, UV1 does show the $1682\,\mathrm{cm}^{-1}$ C=O absorption peak. However, UV2 does not show this band. UV2 does show a peak at a slightly higher wavenumber, at approximately $1686\,\mathrm{cm}^{-1}$. By slightly averaging the UV2 spectrum, as a way to remove the noise in the spectrum, we do observe a peak at approximately $1682\,\mathrm{cm}^{-1}$ (Figure 9). This averaging was performed by using the "MovingAverage" function in Mathematica and letting it compute the moving average of the data by averaging runs of 4 elements. Concerning the $3000-2600\,\mathrm{cm}^{-1}$ region, the UV1 and UV2 spectra do not show any particular broad peak that might indicate OH bonds, similarly to the NI spectrum. A figure of this region is not given.

UV3 and UV4 both show the C=O peak at $1682\,\mathrm{cm}^{-1}$, but for UV3 it is a very small peak. For UV4 the peak is more visible, though it is not as obvious as for the NI sample (Figure 10). However, when we scale the spectra, the whole $1700-1600\,\mathrm{cm}^{-1}$ region of UV3 shows less absorbance than NI (Figure 11a), whereas UV4 shows a slightly higher absorbance (Figure 11b). This scaling is

performed by using the "TwoAxisListLinePlot" function in Mathematica. This functions causes the baselines to coincide as well as the highest points of the spectra, which is the Si – O peak around $1000\,\mathrm{cm}^{-1}$. Again, the $3000 - 2600\,\mathrm{cm}^{-1}$ region does not show any clear OH absorbance bands.

UV5 and UV6 do not show the $1682\,\mathrm{cm}^{-1}$ band, but they do show a peak at a slightly higher wavelength at approximately $1686\,\mathrm{cm}^{-1}$, similar to UV2. Moreover, again when we average these spectra, we can find a peak at $1682\,\mathrm{cm}^{-1}$ (Figure 12). Also, neither of them show anything that might be indicative of OH bands in the $3000 - 2600\,\mathrm{cm}^{-1}$ region.

3.2.3. Amino acids

UV1 and UV2 both show the same $1600\,\mathrm{cm}^{-1}$ peak as the NI sample due to the NH_2 bending absorption (Figure 13a). When scaled, the UV2 absorption is higher than the UV1 absorption (Figure 13b). Similar to NI, UV1 and UV2 do not show any peaks for the NH_2 coupled stretching bands at 1520 and $1350\,\mathrm{cm}^{-1}$. Concerning, the C – N stretching vibration at $1142\,\mathrm{cm}^{-1}$, both the UV1 and the UV2 spectra show this peak with an approximately equal intensity.

UV3 and UV4 both also show a peak at $1600\,\mathrm{cm}^{-1}$, but not the NH_2 coupled stretching bands at 1520 and $1350\,\mathrm{cm}^{-1}$ (Figure 14a). Interestingly, for UV3 the peak is much clearer than for UV4, though the overall spectrum, when scaled, is lower for UV3 than UV4 in the $1700 - 1550\,\mathrm{cm}^{-1}$ region (Figure 14b). Both UV3 and UV4 do not show a peak for the $1142\,\mathrm{cm}^{-1}$ C – N stretching band (Figure 14c). However, they do show some other interesting peaks within the $1250 - 1050\,\mathrm{cm}^{-1}$ region that are not observed for any of the other samples. The C – N stretching vibration is expected to occur between the wavenumbers $1360 - 1080\,\mathrm{cm}^{-1}$. Considering the UV3 and UV4 spectra generally show more of the expected peaks, it is unexpected that they would not show this C – N stretching band. Perhaps, the peak has shifted to slightly lower wavenumbers, as there is for both spectra a peak visible at $1135\,\mathrm{cm}^{-1}$.

The spectra for UV5 and UV6 are quite similar to each other in the $1800 - 1300\,\mathrm{cm}^{-1}$ region (Figure 15a). Both also do clearly show the $1600\,\mathrm{cm}^{-1}$ peak, and again not the NH_2 coupled stretching bands at 1520 and $1350\,\mathrm{cm}^{-1}$. Besides that, both UV5 and UV6 show the C – N stretching peak around $1142\,\mathrm{cm}^{-1}$ (Figure 15b).

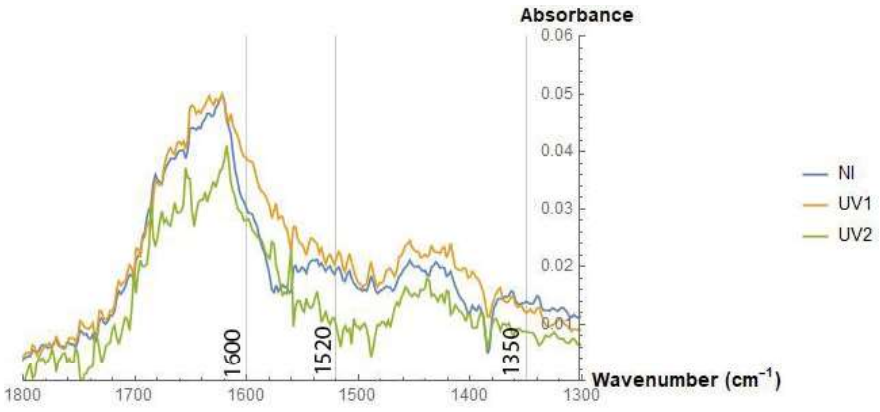

(a) This figure shows the NH_2 bending peak at $1600\,\mathrm{cm}^{-1}$ and where the NH_2 coupled stretching bands are expected to be for the UV1, UV2, and NI spectra.

Figure 13

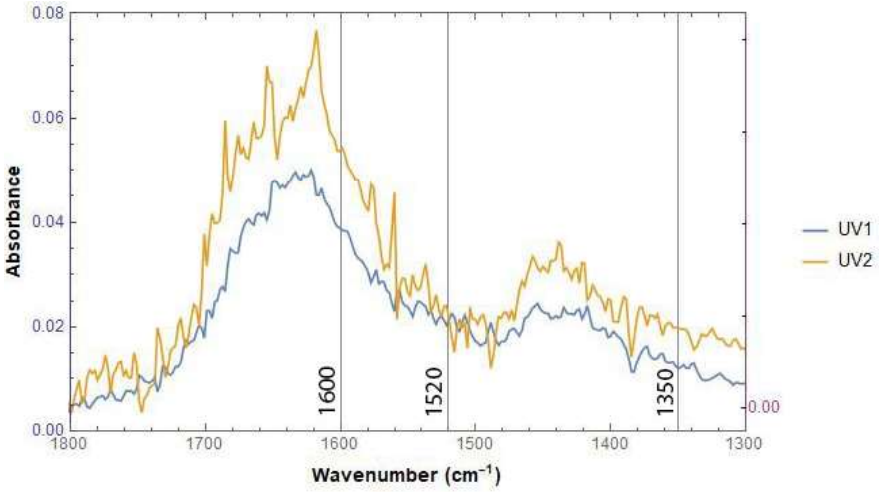

(b) This figure shows the NH_2 bending peak at $1600\,cm^{-1}$ and where the NH_2 coupled stretching bands are expected to be for the scaled UV1 and UV2 spectra.

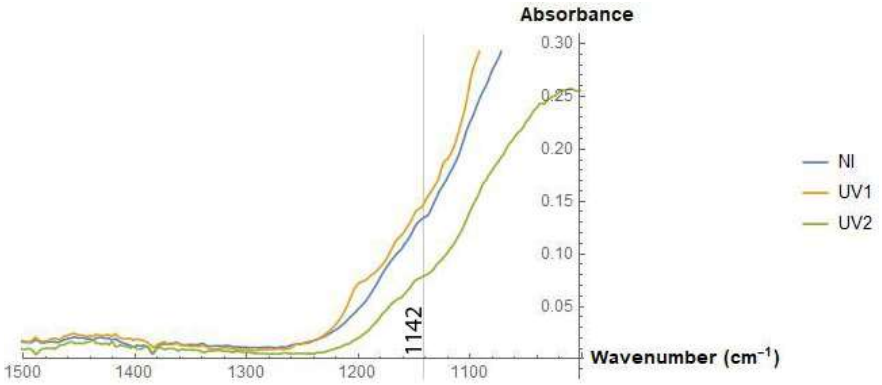

(c) This figure shows the region $(1360 - 1080\,cm^{-1})$ for the UV1 and UV2 spectra, in which we expect to find a band due to the C−N stretching vibration. The peak at $1142\,cm^{-1}$ might be due to this vibration.

Figure 13

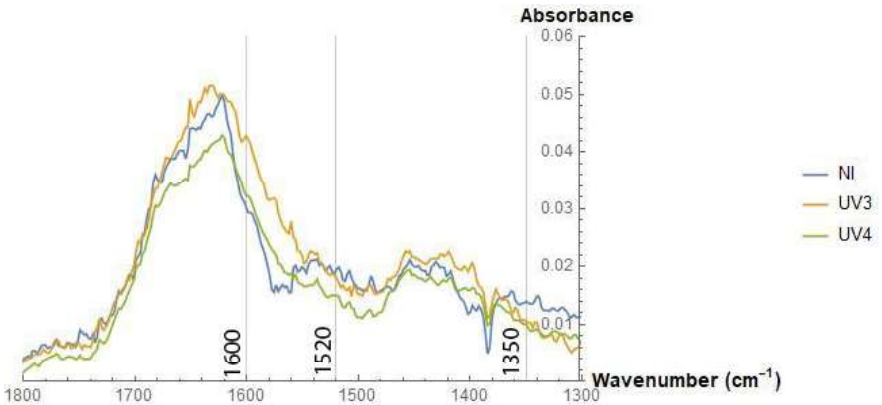

(a) This figure shows the NH_2 bending peak at $1600\,cm^{-1}$ and where the NH_2 coupled stretching bands are expected to be for the UV3, UV4, and NI spectra.

Figure 14

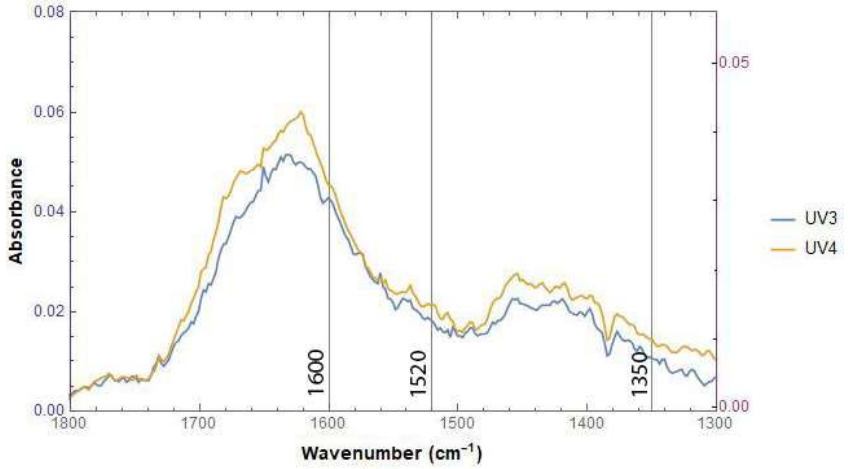

(b) This figure shows the NH_2 bending peak at $1600\,cm^{-1}$ and where the NH_2 coupled stretching bands are expected to be for the scaled UV3 and UV4 spectra.

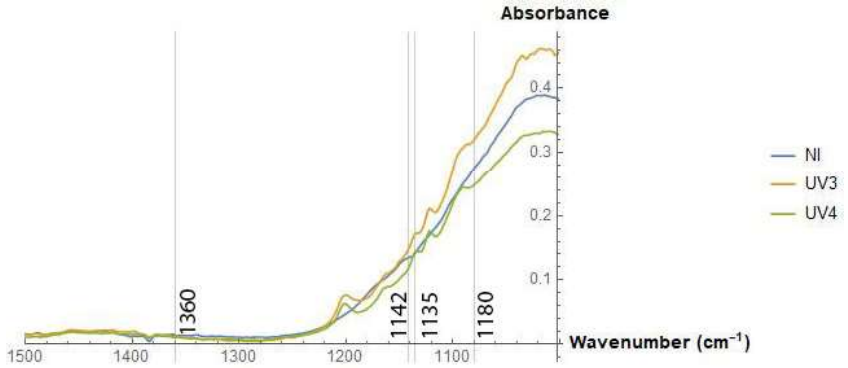

(c) This figure shows the region $(1360 - 1080\,cm^{-1})$ for the UV3 and UV4 spectra, in which we expect to find a band due to the C−N stretching vibration. The peak $1142\,cm^{-1}$ in the NI sample might be due to this, whereas in the UV3 and UV4 samples it might have shifted to a lower wavenumber $(1135\,cm^{-1})$.

Figure 14

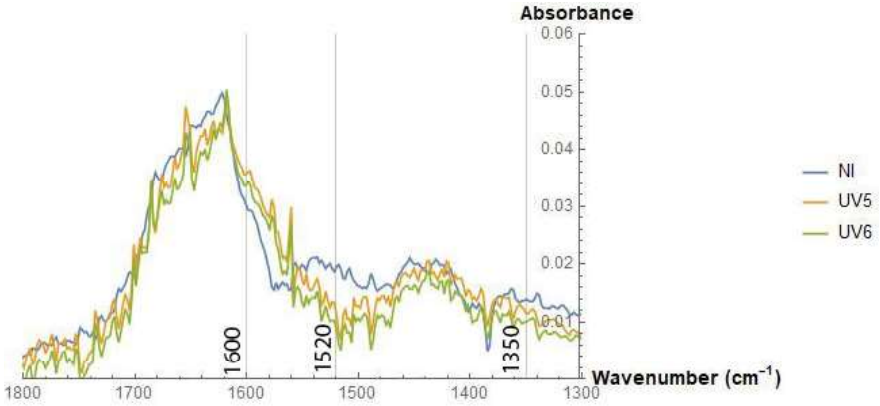

(a) This figure shows the NH_2 bending peak at $1600\,cm^{-1}$ and where the NH_2 coupled stretching bands are expected to be for the UV5, UV6, and NI spectra.

Figure 15

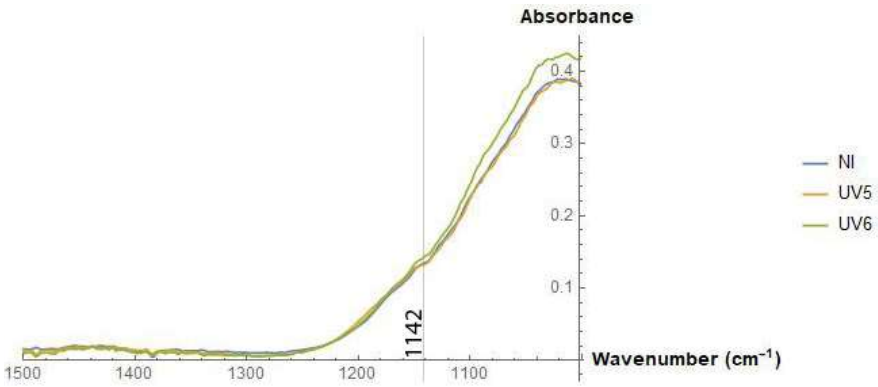

(b) This figure shows the region $(1360 - 1080\,\mathrm{cm}^{-1})$ for the UV5 and UV6 spectra, in which we expect to find a band due to the C−N stretching vibration. The peak at $1142\,\mathrm{cm}^{-1}$ might be due to this vibration.

Figure 15

3.3. Pre-irradiated samples

The results from the FTIR measurements of the pre-irradiated samples, i.e. M1-M4, are combined in Figure 16. In the following section some interesting differences between the NI sample and the M1-M4 samples will be highlighted.

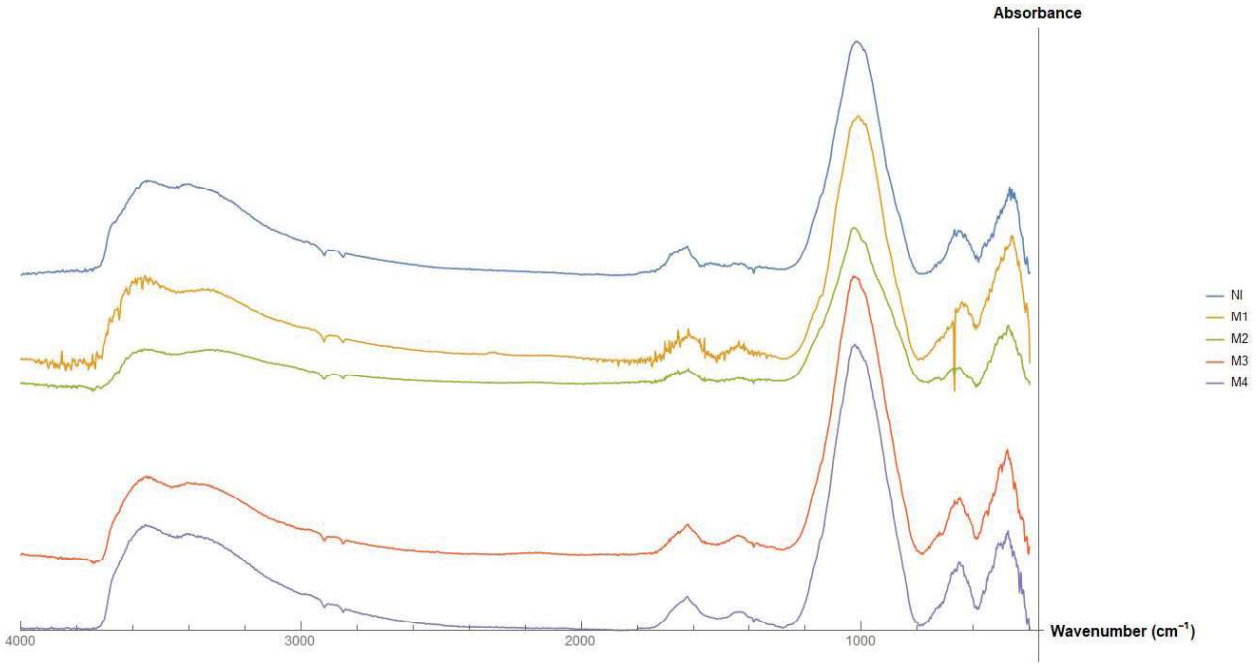

Figure 16: In this figure the complete baseline-corrected IR spectra that followed from the FTIR measurements of samples M1-M4 are stacked on top of each other together with the NI spectrum. The absolute absorbance is therefore not given. The five spectra are given with their absolute absorbance without baseline correction in Figure S5 and with baseline correction in Figure S6.

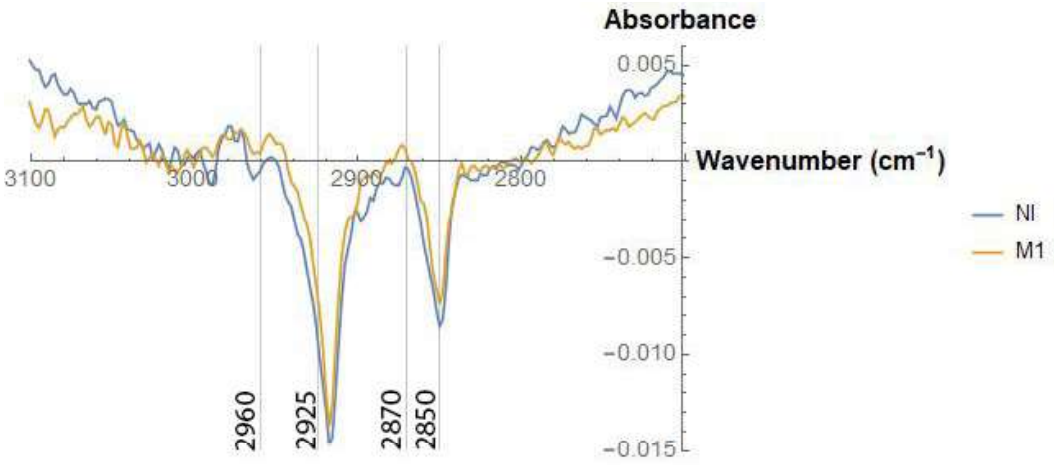

(a)

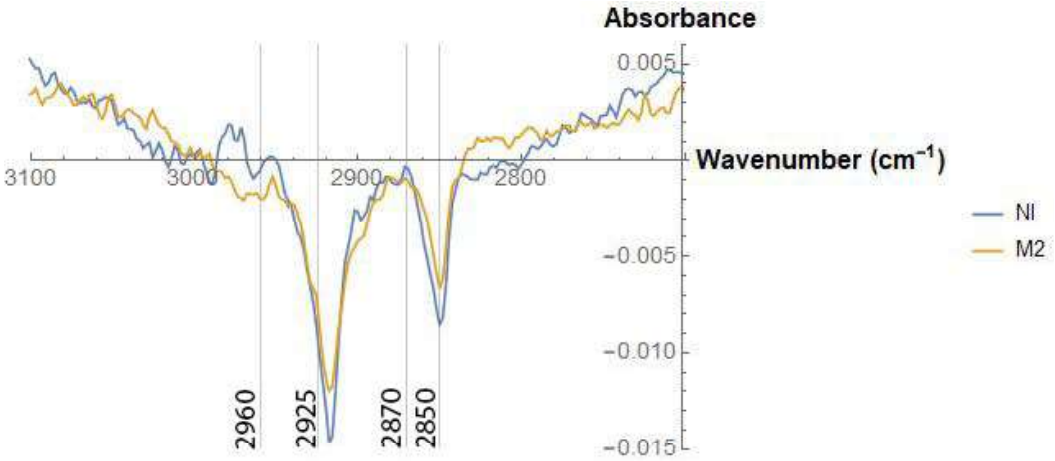

(b)

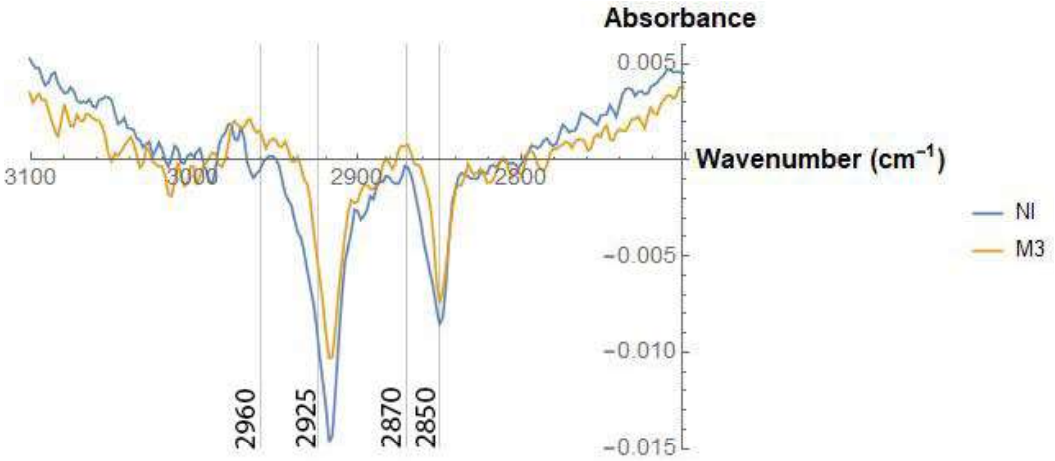

(c)

Figure 17: In these figures the $3100 - 2700\,\mathrm{cm}^{-1}$ region of the M1-M4 and NI spectra are shown together with the 2960 and $2870\,\mathrm{cm}^{-1}$ methyl and 2925 and $2850\,\mathrm{cm}^{-1}$ methylene absorption bands. These spectra were produced by fitting a line to the $3100 - 2700\,\mathrm{cm}^{-1}$ region and subtracting this from the spectrum. *This figure continues on the next page.*

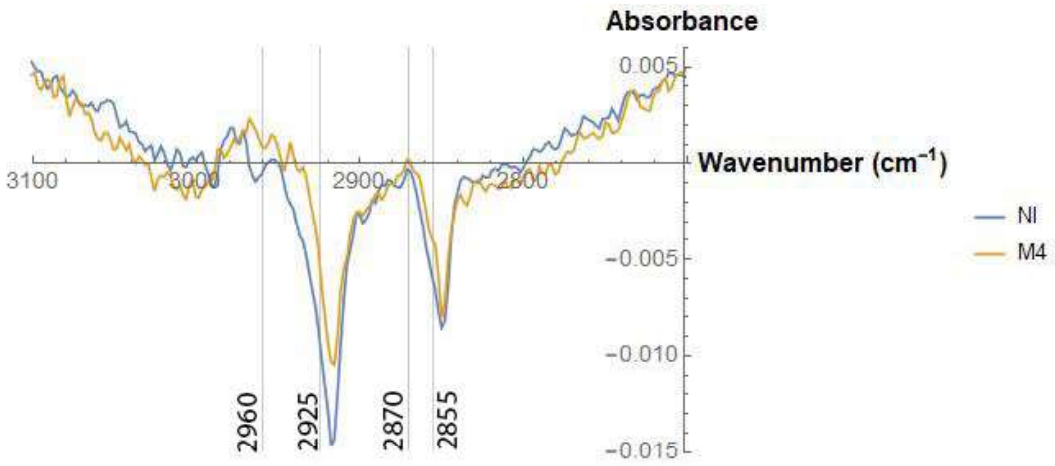

(d)

Figure 17

3.3.1. Hydrocarbons

Figure 17 shows the $3100 - 2700\,\mathrm{cm}^{-1}$ region of the M1-M4 spectra and the NI spectrum with the methyl and methylene absorption bands. The M1 spectrum in this region is quite similar to the NI spectrum. It shows a peak just left and right of the $2960\,\mathrm{cm}^{-1}$ methyl absorption band, though with a lower absorbance than the NI spectrum. The $2870\,\mathrm{cm}^{-1}$ absorption band for methyl is also clearly visible in the spectrum where the fitted line was subtracted. In the regular spectrum it can also be spotted as a very weak peak (this figures is not given here). Neither of the methylene absorption bands are visible in the M1 spectrum.

For the M2 spectrum, there is a very slight peak visible for the $2960\,\mathrm{cm}^{-1}$ methyl absorption band. However, the large peak that was observed to the left of the $2960\,\mathrm{cm}^{-1}$ line for NI and M1 is not visible in this spectrum. The methyl $2870\,\mathrm{cm}^{-1}$ peak can also be observed, though it is weaker than the NI spectrum. The $2850\,\mathrm{cm}^{-1}$ methylene absorption is not observed as it falls right in one of the "background dips" observed in this region of the spectrum. A slight peak can be observed for the $2925\,\mathrm{cm}^{-1}$ methylene absorption band.

The M3 spectrum shows the two peaks left and right from the $2960\,\mathrm{cm}^{-1}$ methyl absorption line, similar to M1 and NI. However, the M3 spectrum also shows another peak exactly at this $2960\,\mathrm{cm}^{-1}$ methyl absorption line. The other methyl band at $2870\,\mathrm{cm}^{-1}$ is also observed and shows a stronger absorbance than the NI sample. Nothing can be observed for any of the methylene bands.

M4 again shows peaks left and right from the $2960\,\mathrm{cm}^{-1}$ methyl absorption line, but none at the exact spot, like M3 did. Moreover, the peak to the left of this line appears different from the ones observed in the M1, M3, and NI spectra. The M4 spectrum does not show any clear methylene bands, though a slight peak can be observed just to the left of the $2850\,\mathrm{cm}^{-1}$ band at approximately $2855\,\mathrm{cm}^{-1}$.

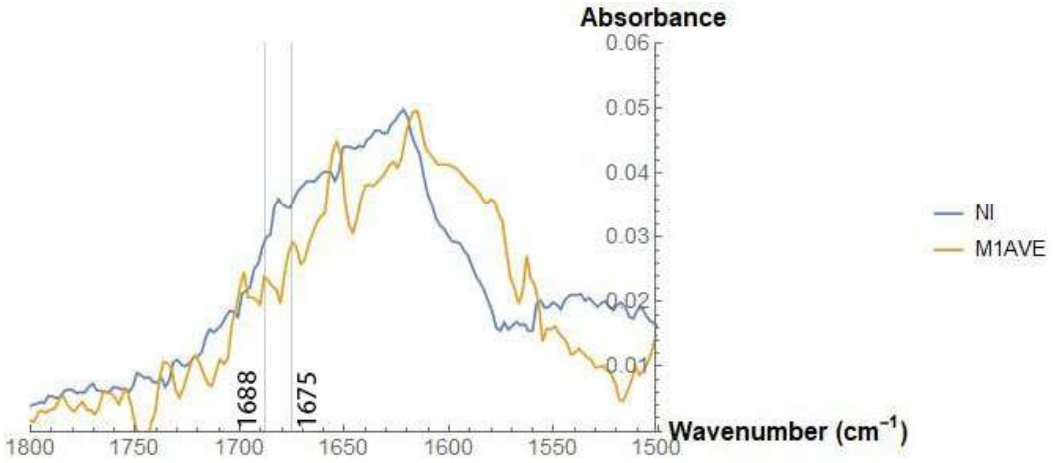

(a)

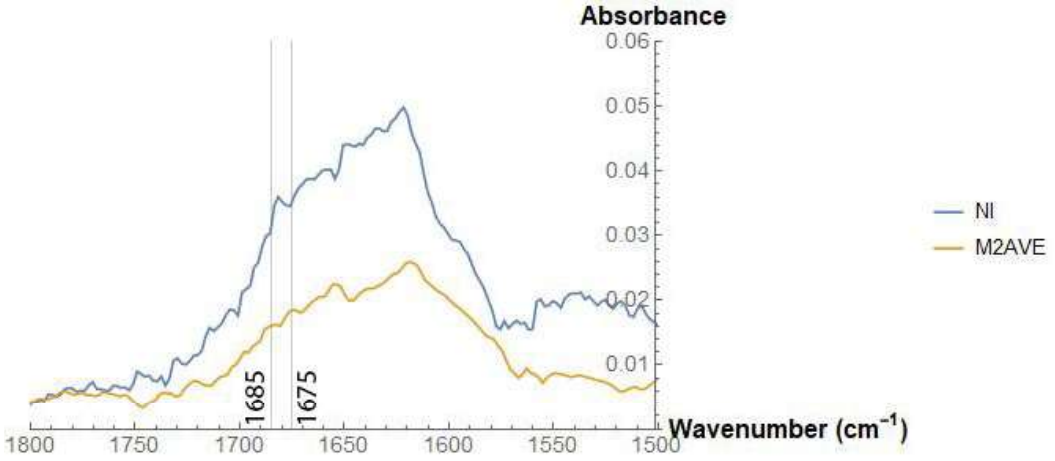

(b)

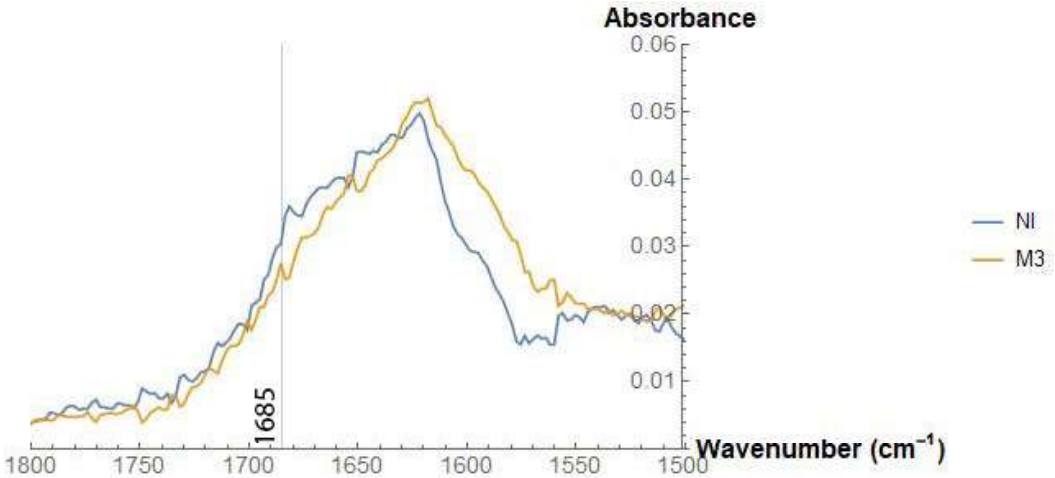

(c)

Figure 18: In this figure the $2000 - 1500\,\mathrm{cm}^{-1}$ region of the M1-M4 and NI spectra is shown. Within the $1760 - 1675\,\mathrm{cm}^{-1}$ range an absorption due to a C=O stretching vibration is expected to be found. In particular, the peak in the NI sample at $1682\,\mathrm{cm}^{-1}$ was assigned to this vibration. *This figure continues on the next page.*

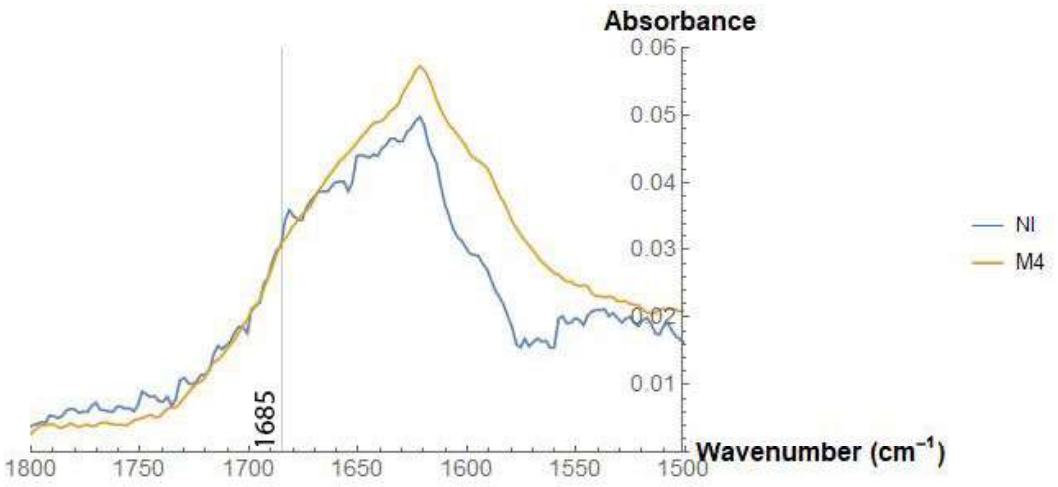

(d)

Figure 18

3.3.2. Carboxylic acids

Figure 18 shows the $2000-1500\,\mathrm{cm}^{-1}$ region of the M1-M4 and NI spectra, in which we expect to find absorptions due to C=O stretching vibrations. M1 has a very fluctuating spectrum in the $2000-1500\,\mathrm{cm}^{-1}$ region, probably due to a change in the atmospheric gases in the FTIR chamber between the background and the M1 spectrum. This makes it quite difficult to distinguish peak from noise. A way through which I have tried to resolve this is again by averaging the M1 spectrum. This does give some peaks in the $1760-1675\,\mathrm{cm}^{-1}$ region. Especially, the peak at $1675\,\mathrm{cm}^{-1}$ might be indicative of C=O stretching, though it has a lower absorbance than the NI spectrum. There are other peaks in the region as well, e.g. at $1688\,\mathrm{cm}^{-1}$.

M2, similar to M1, has a highly fluctuating spectrum in this region. Again by averaging, we find a peak at approximately $1685\,\mathrm{cm}^{-1}$. The $1675\,\mathrm{cm}^{-1}$ peak that was visible in the M1 spectrum is also visible here, though less intense. The non-averaged spectra for the M1 and M2 samples are given in Figure S7 and Figure S8.

The M3 spectrum is less fluctuating and shows a peak at a slightly higher wavenumber than the NI spectrum. Namely, the peak at $1685\,\mathrm{cm}^{-1}$ can be indicative of a C=O stretching absorption.

M4 is the smoothest of all 4 pre-irradiated samples in this region, but it also does not show a clear peak anywhere in the $1760-1675\,\mathrm{cm}^{-1}$ region. Perhaps one slight bump in the spectrum at 1685 could be interpreted as a peak.

Similar to the UV1-UV6 and NI spectra, nothing is visible for the M1-M4 spectra in the $3000-2600\,\mathrm{cm}^{-1}$ OH bonds region, except for the general sloping of the spectrum.

3.3.3. Amino acids

Figures 19 and 20 show the $1800-1300\,\mathrm{cm}^{-1}$ and $1500-1000\,\mathrm{cm}^{-1}$ regions, respectively, of the M1-M4 and NI spectra. For the M1 spectrum again, because of the high amount of fluctuations in this region, the spectrum was averaged. This spectrum also shows the $1600\,\mathrm{cm}^{-1}$ NH_2 bending

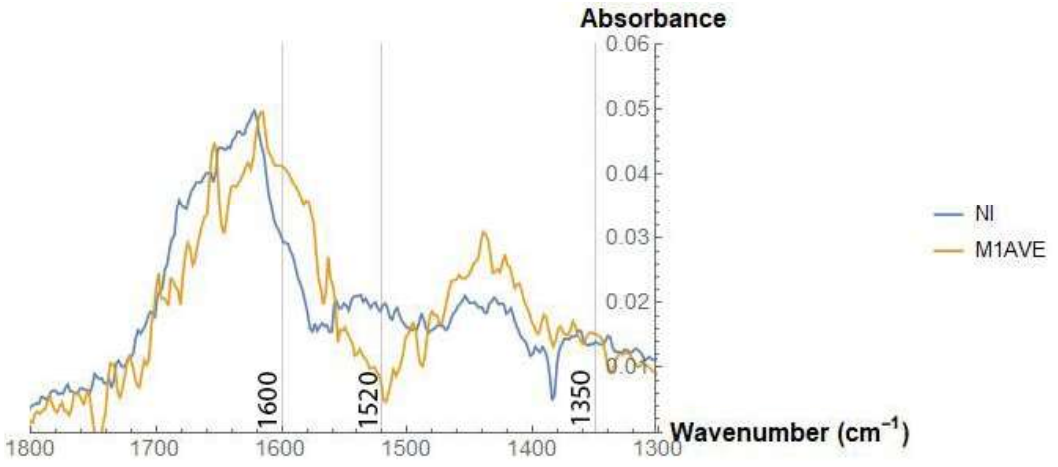

(a)

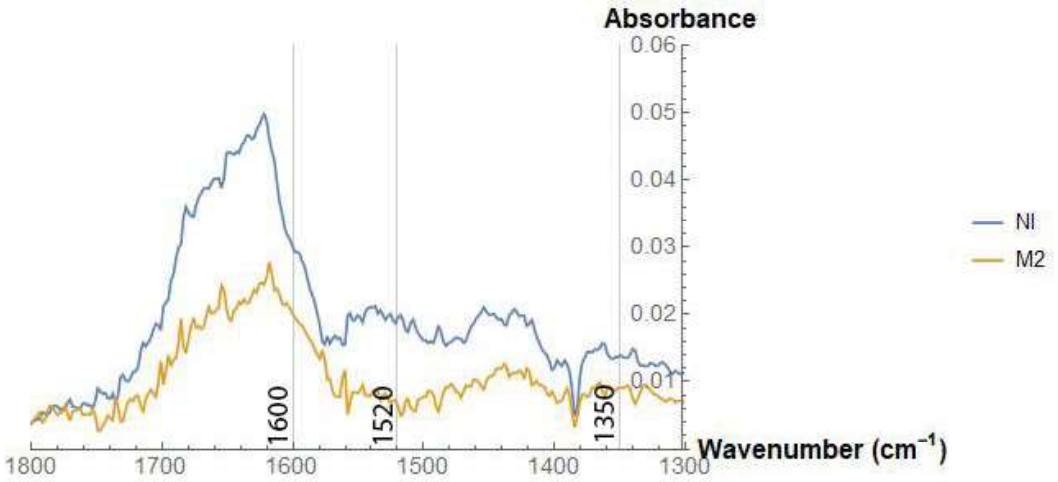

(b)

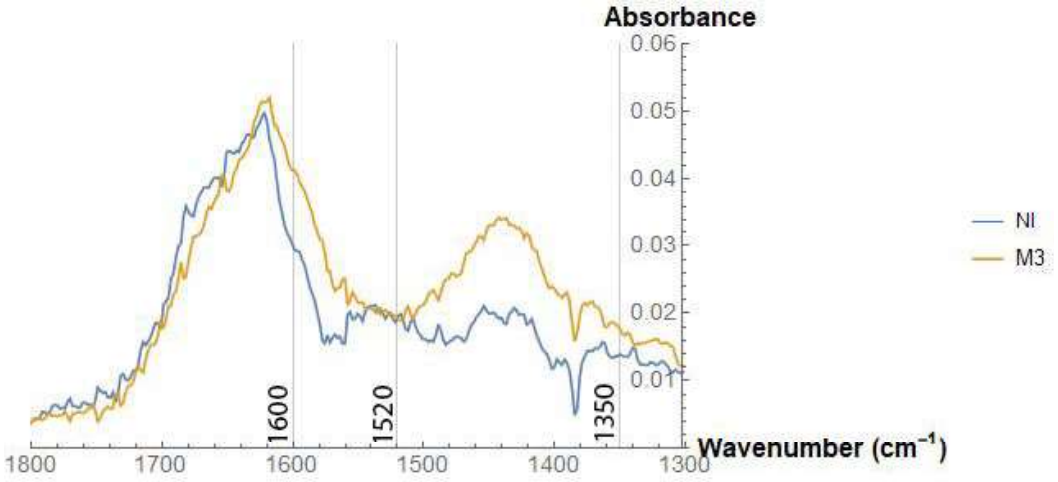

(c)

Figure 19: In this figure the $1800 - 1300\,\mathrm{cm}^{-1}$ region of the M1-M4 and NI spectra is shown. The NH_2 bending absorption at $1600\,\mathrm{cm}^{-1}$ and the NH_2 coupled stretching absorptions at 1520 and $1350\,\mathrm{cm}^{-1}$ are highlighted. *This figure continues on the next page.*

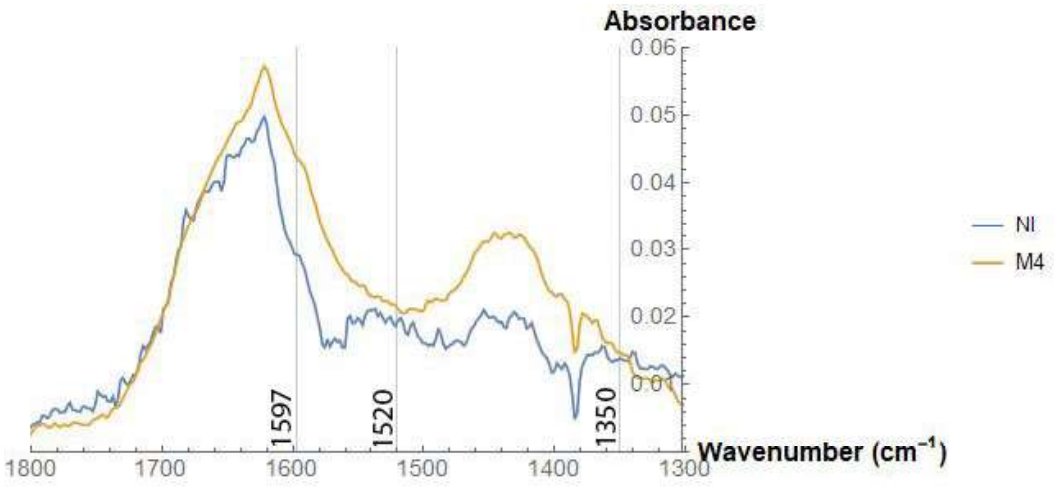

(d)

Figure 19

vibration at a higher absorption than the NI spectrum. At the 1350 cm^{-1} location a peak can also be observed that might be due to the NH_2 coupled stretching vibration, though no peak is observed at the 1520 cm^{-1} location. M1 also shows a peak in the $1360-1080\,cm^{-1}$ C–N stretching region at the same position as the NI spectrum, i.e. at 1142 cm^{-1}. The non-averaged spectra for the M1 sample is given in Figure S9.

The M2 spectrum does not show a clear peak for any of the 1600, 1520, or 1350 cm^{-1} NH_2 absorption bands. The spectrum does clearly show the C–N stretching band at 1142 cm^{-1}.

The M3 spectrum shows a clear peak at the NH_2 bending 1600 cm^{-1} location. It does not show a clear peak for any of the NH_2 coupled stretching absorptions. Again, a clear peak is observed for the 1142 cm^{-1} C–N stretching band.

The M4 spectrum shows a peak slightly to the right from the 1600 cm^{-1} absorption line, at approximately 1597 cm^{-1}. The spectrum does not show any peaks for the NH_2 coupled stretching absorptions, and again it does show a clear peak for the 1142 cm^{-1} C–N stretching band.

4. Discussion

A decrease in the organic content of the Murchison sample was expected, as UV radiation is known to cause degradation of organic compounds. This degradation can occur through two different mechanisms. First, UV radiation can cause direct photolysis as the molecules absorb UV photons. Besides that, the UV can also cause a reaction with oxidizing species that are present in the atmosphere (Hintze, Buhler, Schuerger, Calle, & Calle, 2010). The first mechanism requires the compound in question to absorb in the UV range, which is not always the case. OH radicals are produced as a result of high UV radiation in the presence of water. The UV5 and UV6 samples had added water and it would be expected that they might show an increased effect due to the UV radiation. However, there was no indication of the presence of any OH significantly different from the UV1-UV4 spectra. Moreover, compared to the UV1-UV4 samples, no increased effect from the UV radiation was observed for samples UV5 and UV6. UV radiation can lead to both

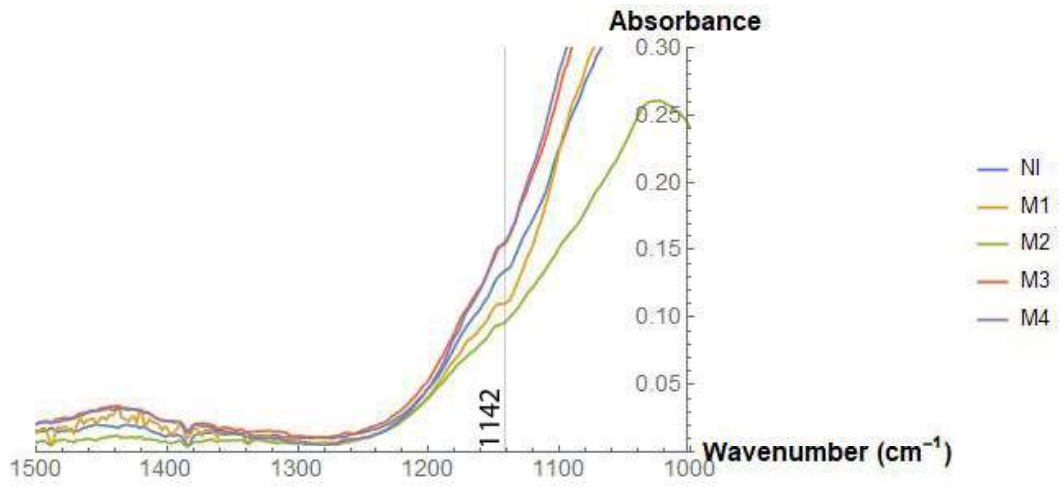

Figure 20: In this figure the $1500-1000\,\mathrm{cm}^{-1}$ region of the M1-M4 and NI spectra is shown. The C–N stretching absorption at $1142\,\mathrm{cm}^{-1}$ is highlighted.

fragmentation of the organic compounds to molecules with a lower molecular weight, e.g. CO_2 and CH_4, or compounds with a higher molecular weight can be formed. These structures with a higher molecular weight can show a higher photostability to UV radiation (Poch, Kaci, Stalport, Szopa, & Coll, 2014).

Though the quantitative aspects of UV degradation of organics is an interesting and important matter, for example in order to get a grasp of the timescales over which organics are degraded on the Martian surface as Poch et al. (2014) pointed out, no such thing could be achieved in this research. The spectra are too complex with too many overlapping peaks to be able to draw any concrete quantitative conclusions from the data. Quantitative analyses of organic UV degradation have been performed on pure organic samples (Poch et al., 2014), though their results still had a large confidence interval. Quantitative analysis is also limited in this research as the thickness of the samples in the cups was not measured or actively controlled for. UV radiation interacts with the first millimeter of the sample, hence an optically thin sample in the range of $190-400\,\mathrm{nm}$ would be required for quantitative analysis (Poch et al., 2013). The UV1, UV2, UV5, and UV6 samples were prepared to be as thin as possible, though no measurement of their thickness was made. UV3 and UV4 filled up the entire sample cup as they were already KBr mixed and hereafter directly measured in the FTIR.

4.1. Hydrocarbons

Looking at the 2850 and $2925\,\mathrm{cm}^{-1}$ methylene and the 2870 and $2960\,\mathrm{cm}^{-1}$ methyl peaks, some interesting differences can be observed between the spectra. However, it is worth noting that any peaks were generally difficult to distinguish in this region due to noise and the general slope of the spectrum in this region[1].

First, concerning the methylene absorption lines, these were generally hardest to distinguish, because of the two dips that occurred in most of the spectra. The $2850\,\mathrm{cm}^{-1}$ is actually barely

[1]The spectra that were compared in order to make the deductions given below, were compared by scaling the spectra as described before.

visible in the NI spectrum, but can be seen as a very small bump in the spectrum at approximately 2854 cm^{-1}. In the other spectra where this peak can also be observed (UV1, UV2, UV4, UV6, M4), it also occurs just left of 2850 cm^{-1}, at approximately 2854 cm^{-1}. It is definitely interesting that this methylene peak does occur in the UV4 and UV6 spectra, which were located in the "night-time" area of the UV irradiation chamber and not exposed to UV radiation, and that the same peak is not visible in the UV3 and UV5 spectra, which were placed in the "day-time" area of the chamber and hence exposed to UV radiation. We might expect the same for the UV1 and UV2 pair, but we do see the same peak in UV1, though it is very slightly weaker than UV2, which might as well be due to noise. The fact that M4 does show the peak, whereas M1-M3 do not, also supports the idea that the UV radiation is causing the methylene abundance to decrease in the meteorite powder, as M4 was one of the samples that received the lowest amount of radiation. One of the reasons that UV1 might still show the peak is that this sample was mixed after irradiation and the unaffected part of the sample from the bottom of the sample cup might be causing this peak, whereas UV3 was put directly into the FTIR. However, then it would be expected for UV5 to also show a peak, whereas it does not.

The other methylene peak, at 2925 cm^{-1}, also provides a strong case that the UV radiation is breaking down methylene bonds in the sample. This peak is not present in the UV1 and UV5 samples, which were exposed to UV radiation. It is present in UV3, which was also exposed to UV radiation, but when comparing it to the same peak in UV4 it appears significantly weaker in UV3 (Figure 7b). The peak is also visible in the UV2 spectrum and weakly in the UV6 spectrum. Combined, this shows that the peak does occur in spectra of samples that were not exposed to UV radiation, and does not occur (as strong) in samples that were exposed to UV radiation. Interestingly, this peak was not observed in the NI spectrum. And even more curiously, the peak *is* observed in the M2 spectrum, which received approximately half as much radiation as the UV1, UV3, and UV5 spectra but over twice as much time. Moreover, the peak is not visible in the M3 and M4 spectra, which received substantially less radiation than M2. And below we will also see that the methyl peaks for M2 are barely to not visible, indicating substantial influence from UV radiation on the hydrocarbons in the sample.

The influence of UV radiation on the methyl absorption peaks is not as obvious as for the methylene absorption peaks. The 2870 cm^{-1} peak is approximately equal for the UV3 and UV4 spectra. The peak is slightly stronger in the UV2 spectrum than the UV1 spectrum, and there is an even more slight difference between the UV5 and UV6 spectra, with UV6 having the stronger absorption. So again we see a decrease of methyl abundance in this peak under the influence of UV radiation, though the effects seem less strong than for the methylene peaks. For the M1-M4 samples, the peak appears weakest in the M2 spectrum, somewhat stronger in the M1 spectrum, and strongest in the M3 and M4 spectra, which have an approximately equal absorption. We would expect the M1 sample to have the lowest absorption, as it received much more radiation and over a longer time than M2. And as mentioned above, the fact that M2 shows this methyl peak so weakly, but does show the 2925 cm^{-1} methylene peak is contradicting.

The 2960 cm^{-1} methyl peak shows the same pattern for the M1-M4 samples. This peak is absent in the M2 spectrum, slightly visible in the M1 spectrum, and appears more strongly in the M3 and M4 spectra. For the UV1-UV6 spectra, no real difference can be seen for the UV1 and UV2 pair or the UV5 and UV6 pair. UV4 does clearly show a much higher absorbance than UV3. Again, the visibility of this difference in UV4 and UV3, but not in the other pairs, might be due to the immediate FTIR measurement performed on the UV3 and UV4 samples, whereas the others

still had to be mixed with KBr. Together this again implies a decrease in abundance of methyl groups under the influence of UV radiation, though the M2 spectrum does not conform to the general trend.

Hintze et al. (2010) looked at the effects of UV radiation on octadecane ($C_{18}H_{38}$) and phenanthrene ($C_{14}H_{10}$) as to represent the aliphatic hydrocarbons and PAHs present in meteorites, though octadecane and phenanthrene themselves are only present in trace amounts. They found that octadecane does not absorb UV radiation strongly, so degradation of this compound would likely not be due to direct absorption of UV radiation. On the other hand, phenanthrene does absorb strongly in the UV region of the electromagnetic spectrum. However, for both compounds they did not observe any differences between the control and irradiated sample in the IR spectrum. Hintze et al. (2010) also did conclude that infrared spectroscopy does not have sufficient sensitivity to differentiate between reaction products of octadecane pyrolysis and octadecane itself.

Poch et al. (2014) researched the UV effects on chrysene ($C_{18}H_{12}$), a polycyclic aromatic hydrocarbon (PAH), which is one of the most abundant PAHs in carbonaceous chondrites. In the infrared spectra of the pure chrysene samples they found a decrease in intensity of the infrared bands and that these bands conserved their shapes, but no appearance of any new bands that might be associated with solid photoproducts of the UV degradation. This would indicate that the photoproducts are mainly volatile. We did not find any new bands associated with photoprodocts in our infrared spectra either.

4.2. Carboxylic Acids

The identified $1682\,\mathrm{cm}^{-1}$ C=O stretching band shows a decrease in absorbance for the UV1 and UV3 samples when compared to the UV2 and UV4 samples, respectively. The UV5 and UV6 samples, however, do not show any significant differences in their spectra in this area. The M1-M4 spectra are even less evident in any effects they might show due to the UV radiation. The M4 spectrum does not even show any apparent peak at $1682\,\mathrm{cm}^{-1}$, though the absorbance is stronger in that region than for the M3 spectrum. The peak observed in the M3 spectrum is stronger than the one in the M2 spectrum, which again is stronger than the one in the M1 spectrum, though the differences are slight.

As mentioned before, the $3000-2600\,\mathrm{cm}^{-1}$ C–H stretching region does not show any peaks for any of the spectra, and thus no information can be deduced from this region for these bands.

Hintze et al. (2010) looked at the effects of UV radiation on octadecanoic acid ($C_{18}H_{36}O_2$) and benzoic acid (C_7H_6O) as to represent the carboxylic acids present in meteorites, though octadecanoic acid and benzoic acid themselves are only present in trace amounts. They found that octadecanoic acid does not absorb UV radiation strongly, so degradation of this compound would likely not be due to direct absorption of UV radiation. Benzoic acid does absorb strongly in the UV region. They did not observe any differences between the control and irradiated sample in the IR spectrum for octadecanoic acid. On the other hand, they did observe some changes in the IR spectrum of benzoic acid. However, in our IR spectra we do not observe similar changes. Hintze et al. (2010) find that new OH features appear around $3500\,\mathrm{cm}^{-1}$, whereas the OH features that we observe occur around $3350\,\mathrm{cm}^{-1}$. This OH peak seems to not be present in the NI sample (in this spectrum there is a peak, but centered at $3405\,\mathrm{cm}^{-1}$), whereas is does appear in the UV1-UV6

samples, where the "day" samples show a stronger peak than the "night" samples for the UV1-UV4 samples. The UV5 and UV6 samples do not show any considerable difference. The M1 and M2 spectra also show this 3500 cm^{-1} peak, but the M3 and M4 spectra are more similar to the NI samples. This all indicates the production of more OH groups as also observed by Hintze et al. (2010), though it is not observed at the same wavenumbers in our research.

4.3. Amino Acids

For the signature amino acid peaks, the 1600 cm^{-1} peak shows the most interesting effects. The UV2 spectrum shows a stronger peak than the UV1 spectrum, indicating a decrease of amino acid content due to the effects of UV radiation. Besides that, the area in which amino acid peaks are found ($1700-1550\,cm^{-1}$) is generally decreased for the UV1 spectrum in comparison the the UV2 spectrum, relatively to the rest of the spectra. For the UV3 and UV4 spectra we see the same effect, namely that the $1700-1550\,cm^{-1}$ area shows less absorbance for the UV3 spectrum than the UV4 spectrum. However, the peak at 1600 cm^{-1} appears to be stronger for the UV3 spectrum than for the UV4 spectrum in comparison to the rest of that region. There is no real difference observed between the UV5 and UV6 spectra. Concerning the M1-M4 spectra, the M2 spectra does not show any peak at all. The M1 spectra does show a peak at 1600 cm^{-1}, but there is also a lot of noise observed in that region stronger than this peak, so there is a good change the peak is also due to noise. For the M3 and M4 spectra, obvious peaks can be distinguished at 1600 cm^{-1}, and the M4 spectrum shows a higher absorbance than the M3 spectrum. This also conforms to the theory that the amino acid content decreases as the M3 sample experienced a higher UV intensity than M4 did. It is curious that the UV5 and UV6 spectra are so similar to each other in this region. Moreover, for the hydrocarbons we found that the UV3 and UV4 spectra demonstrate the difference between the irradiated and non-radiated sample better than the other samples, likely due to the immediate FTIR measurement. However, for the 1600 cm^{-1} the effects are less evident for the UV3 and UV4 spectra than for the UV1 and UV2 spectra.

For the NH_2 coupled stretching bands at 1520 and 1350 cm^{-1} most spectra do not show any bands. Only for the UV3 and UV4 spectra some small peaks can be observed. Especially for the 1520 cm^{-1} location a peak can be observed that appears slightly stronger for the UV4 spectrum than the UV3 spectrum. Though this also indicates a decrease in amino acid content under the influence of UV radiation, only one group of the samples shows this effect and the effect observed there is not at all strong.

The C–N stretching vibration at 1142 cm^{-1} does not show any significant differences between the UV1 and UV2 spectra or the UV5 and UV6 spectra. The UV3 and UV4 spectra do not show any peaks at the exact 1142 cm^{-1} location, but they do at a slightly lower wavenumber, at approximately 1135 cm^{-1}. At this wavenumber the absorbance is slightly lower for UV3 than for UV4. For the M1-M4 spectra we do observe the peaks at 1142 cm^{-1} as well as some differences between the spectra. The absorbance for M3 and M4 is approximately equal and slightly lower for M1 and lower again for M2. This is a curious result as we would expect M1 to show a lower absorbance than M2 as it received a much higher intensity of UV radiation.

The effects of UV radiation on amino acid stability has been researched by Stoker and Bullock (1997). They researched the change in glycine content as the consequence of UV irradiation with a broad spectrum Xenon lamp. They found that as a consequence of this radiation the glycine

content decreased at a rate that would exceed the accumulation of organics through exogenous delivery, hence the non-detection of organics on the Viking mission. Their conclusion supports the theory that we indeed observe a decrease in amino acid content under the influence of UV radiation, though (Stoker & Bullock, 1997) irradiated for a longer time (5 weeks instead of the 24 hour duration of our experiment). Poch et al. (2014) also researched the effects of a Martian UV flux on a pure glycine sample and found that glycine has a half-life of the order of tens to hundreds of hours (ranging from 300 ± 230 h to 330 ± 280 h). Known photoproducts of glycine are CO_2 and CH_4. Poch et al. (2014) also observed polymerization of glycine under the influence of UV radiation, as did Poch et al. (2013). Poch et al. (2013) found this through the appearance of a new broad absorption in the $3600 - 3000\,\mathrm{cm}^{-1}$ range, which was centered around $3250\,\mathrm{cm}^{-1}$, indicative of OH groups. As mentioned before, a similar feature was observed in the samples centered around $3300\,\mathrm{cm}^{-1}$. Poch et al. (2013) suggest that these OH groups appear through the production of water molecules via the polymerization and peptide bond formation between glycine molecules. Other suggestion they make for photoproducts include methanoic acid, acetic acid, and glycolic acid.

5. Conclusion

For all organic compounds that were examined in this research, i.e. hydrocarbons, carboxylic acids, and amino acids, the general trend observed was that the UV radiation caused a decrease of the organic compound in the Murchison sample. This effect was generally better observed in the UV1-UV6 samples, where it was a clear distinction between a sample that was irradiated and a sample that was not irradiated. For the M1-M4 samples, the effects were harder to observe between the various degrees of radiation intensity and duration. Especially the M2 spectrum did not conform to the general trend that could be observed in the M1-M4 samples. Moreover, the M3 and M4 spectra often appeared quite similar to each other, probably due to the fact that M4 received a lower radiation intensity than the M3 sample, but over a longer time.

The UV5 and UV6 spectra did not show any increased effects when compared to the UV1-UV4 spectra. An increased effect was expected due to the addition of H_2O droplets to the sample, which can form OH radicals under the influence of UV radiation. These radicals can also interact with the organics in the sample and cause their destruction. However, no significantly different OH features were observed for the UV5 and UV6 samples, compared to the UV1-UV4 samples. The UV3 and UV4 spectra did generally show stronger effects of the UV radiation than the other samples we irradiated. This indicates that mixing the Murchison sample with KBr before irradiating does give better results, because the sample was not mixed afterwards anymore as happened for the UV1, UV2, UV5, and UV6 samples, causing the part of sample that was at the bottom of the sample holder and thus receiving less radiation to mix with the fully affected upper part.

Though this method is able to show that the organic content of the meteorite sample has decreased, it is not helpful in trying to deduce any quantitative information. Besides only being able to provide qualitative information with some certainty, the qualitative information that it gives is not very in depth. Because the infrared spectra are so complex, due to the many different kinds of compounds that are present in the samples, the overlapping peaks make it difficult to distinguish between them and to accurately and confidently attribute them to the correct molecular bound causing them. Other researches generally consider one particular kind of organic compounds, such as

amino acids, and perform an extraction of amino acids, such that only those appear in the infrared spectrum (Lawless, 1973). This can make the destructive effects of the UV radiation much clearer as well as allow a better identification of possible photoproducts that were created due to the UV radiation. Perhaps the method in this research can be used as an initial measurement, to observe the general effects and identify where potential effects due to UV occur to determine how to proceed.

Supplemental Figures

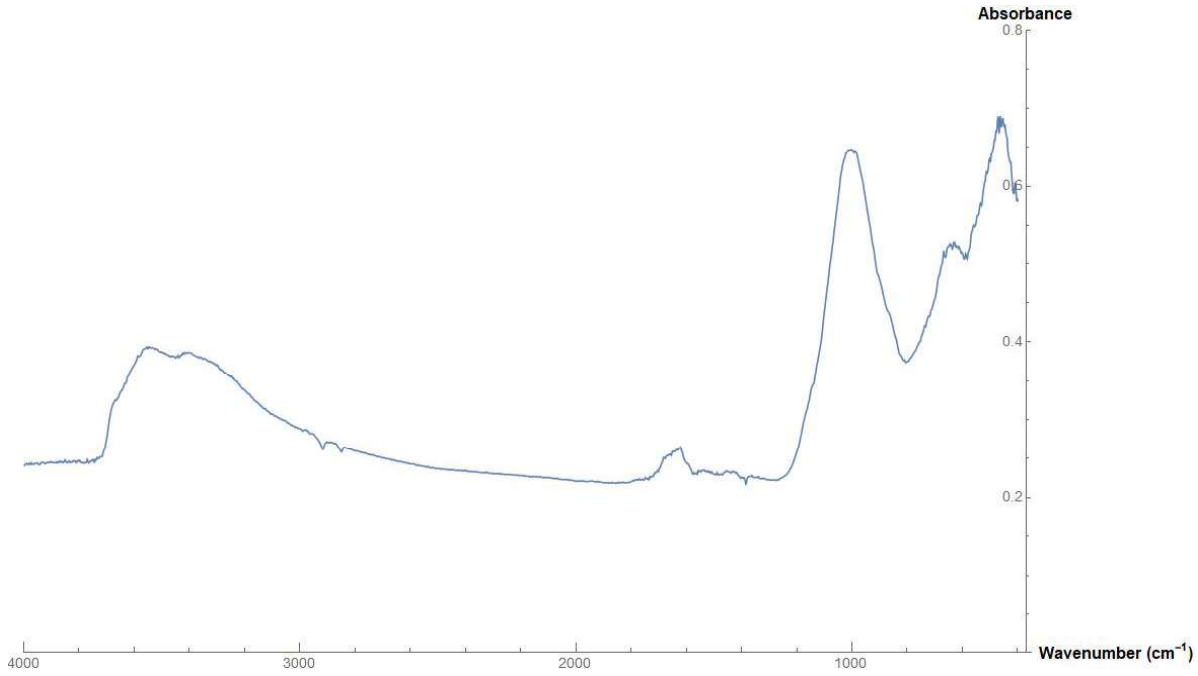

Figure S1: In this figure the IR spectrum that followed from the FTIR measurement without any baseline correction of the NI sample is shown.

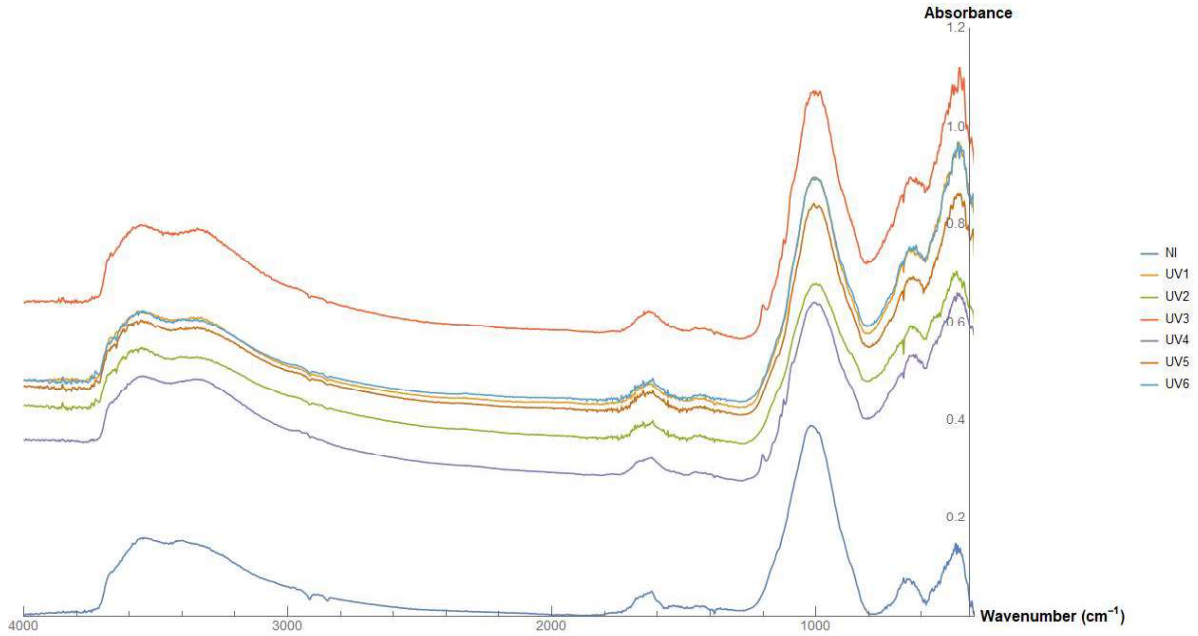

Figure S2: In this figure the IR spectra that followed from the FTIR measurements without any baseline correction of samples UV1-UV6 are shown with their absolute absorbance.

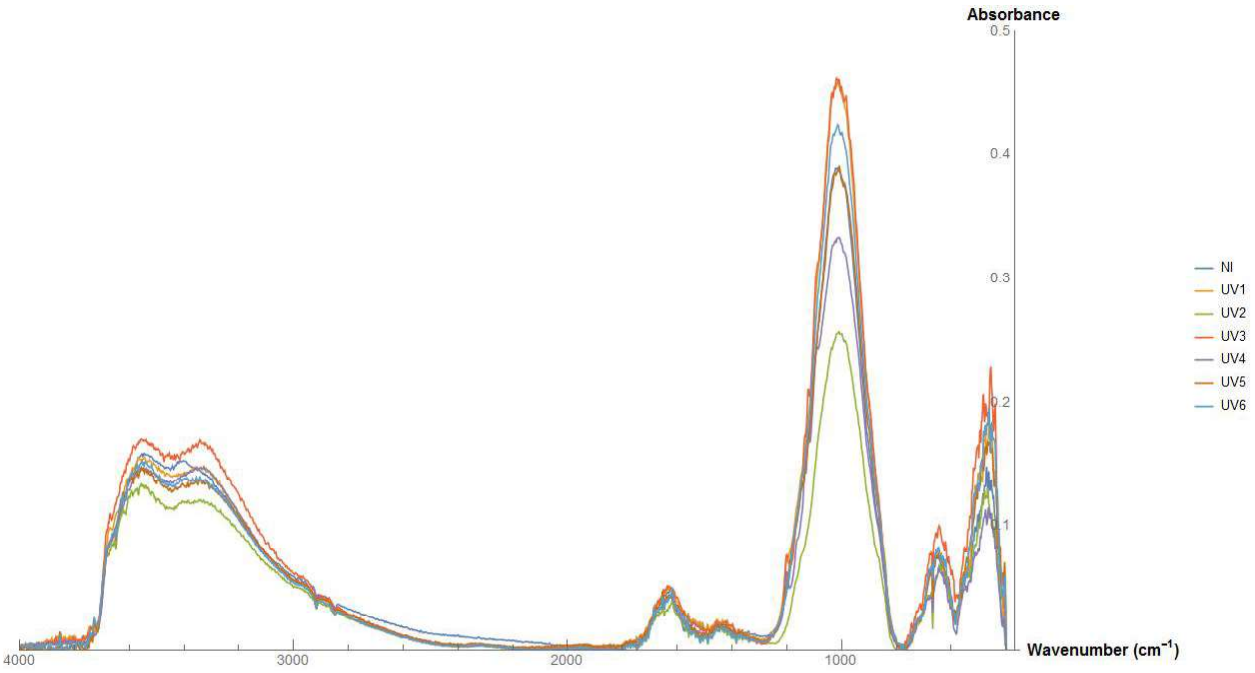

Figure S3: In this figure the complete baseline-corrected IR spectra that followed from the FTIR measurements of samples UV1-UV6 are shown with their absolute absorbance.

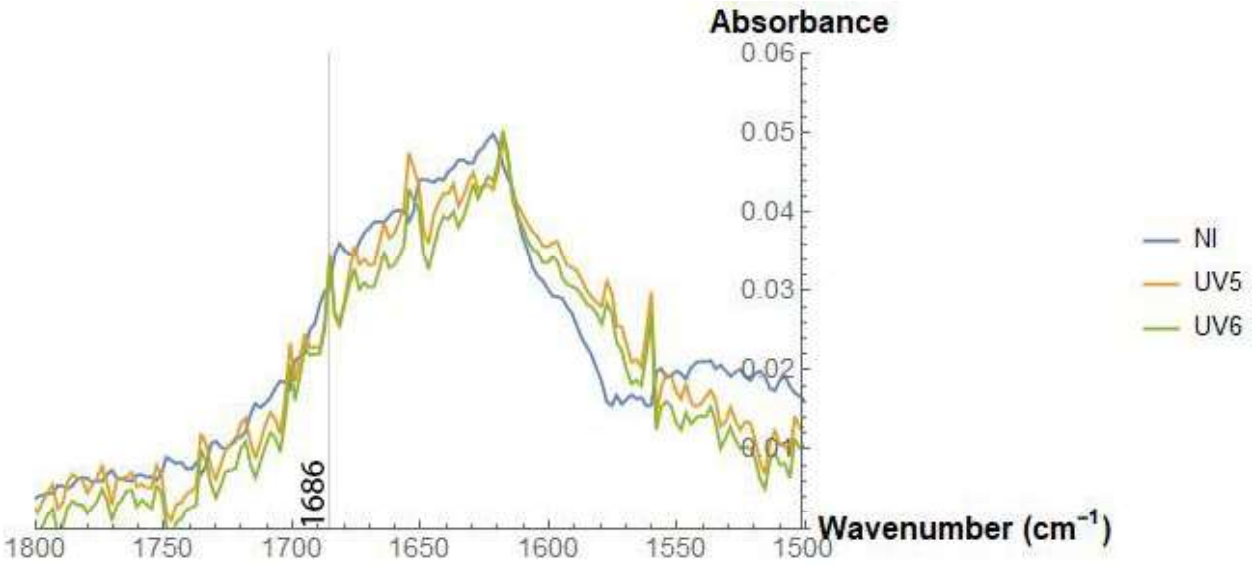

Figure S4: This figure shows the C=O absorption region of the UV5 and UV6 spectra, and the NI spectrum. In particular, the peak at approximately 1686 cm^{-1} might be due to the C=O stretching absorption.

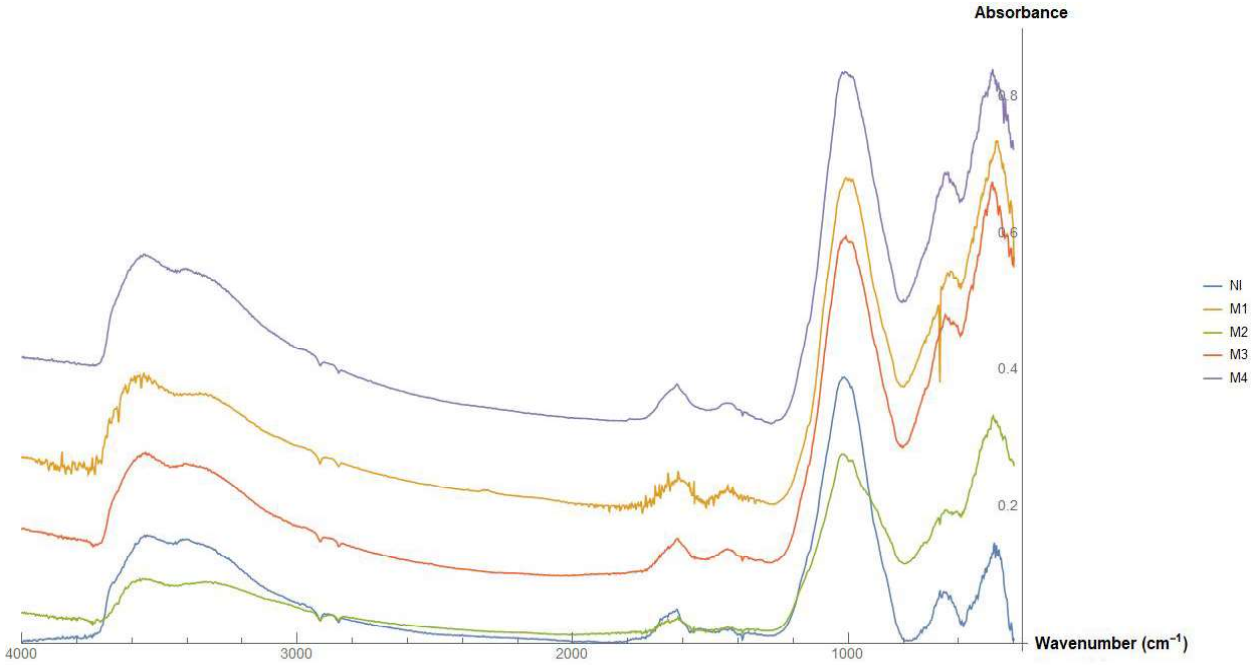

Figure S5: In this figure the IR spectra that followed from the FTIR measurements without any baseline correction of samples M1-M4 are shown with their absolute absorbance.

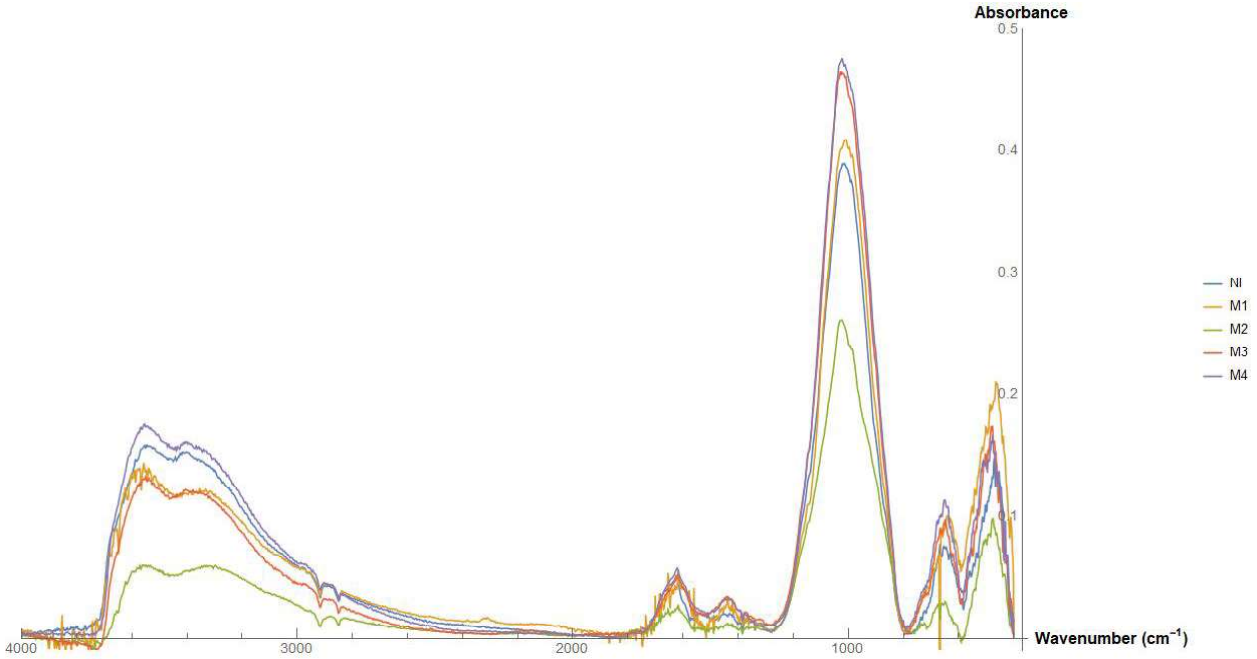

Figure S6: In this figure the complete baseline-corrected IR spectra that followed from the FTIR measurements of samples M1-M4 are shown with their absolute absorbance.

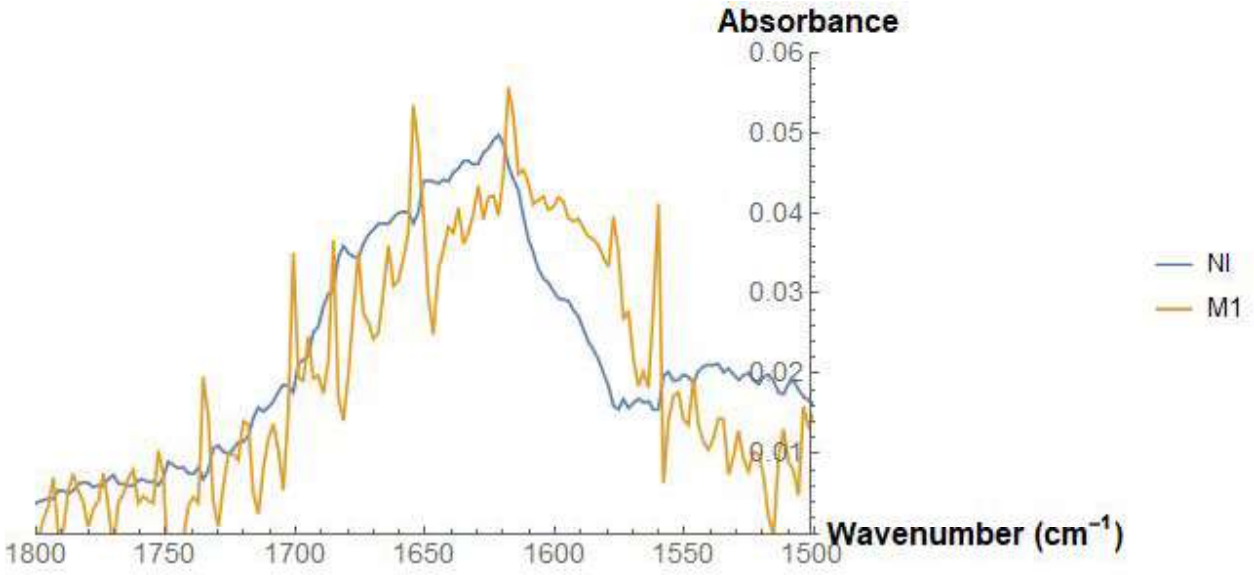

Figure S7: This figures shows the non-averaged spectrum of the M1 and NI sample for the $1800-1500\,\mathrm{cm}^{-1}$ region.

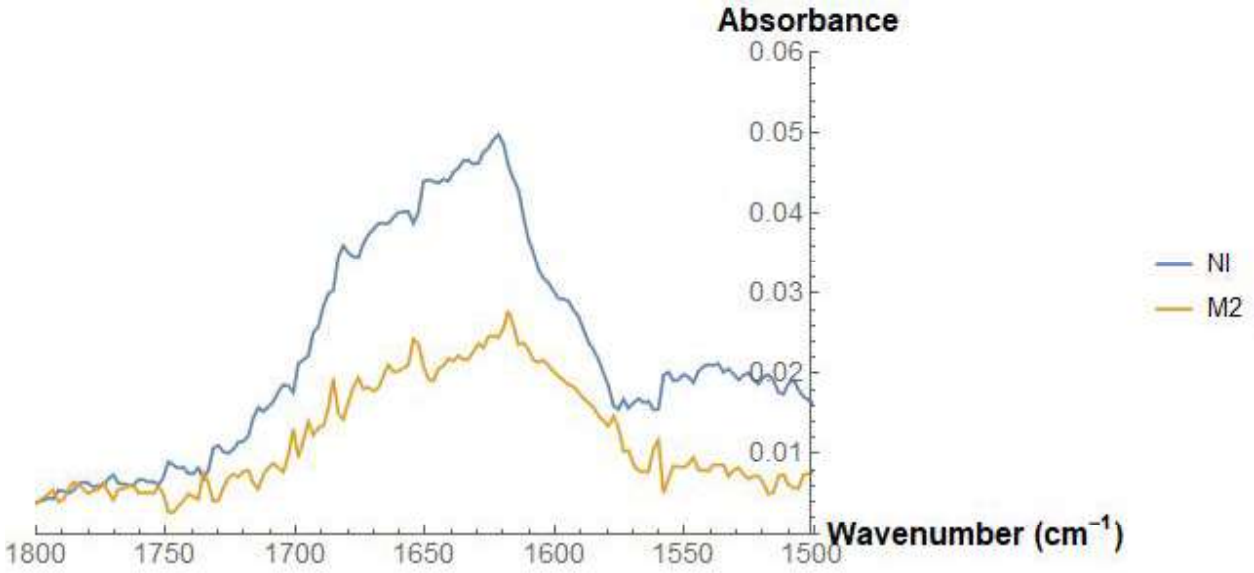

Figure S8: This figures shows the non-averaged spectrum of the M2 and NI sample for the $1800-1500\,\mathrm{cm}^{-1}$ region.

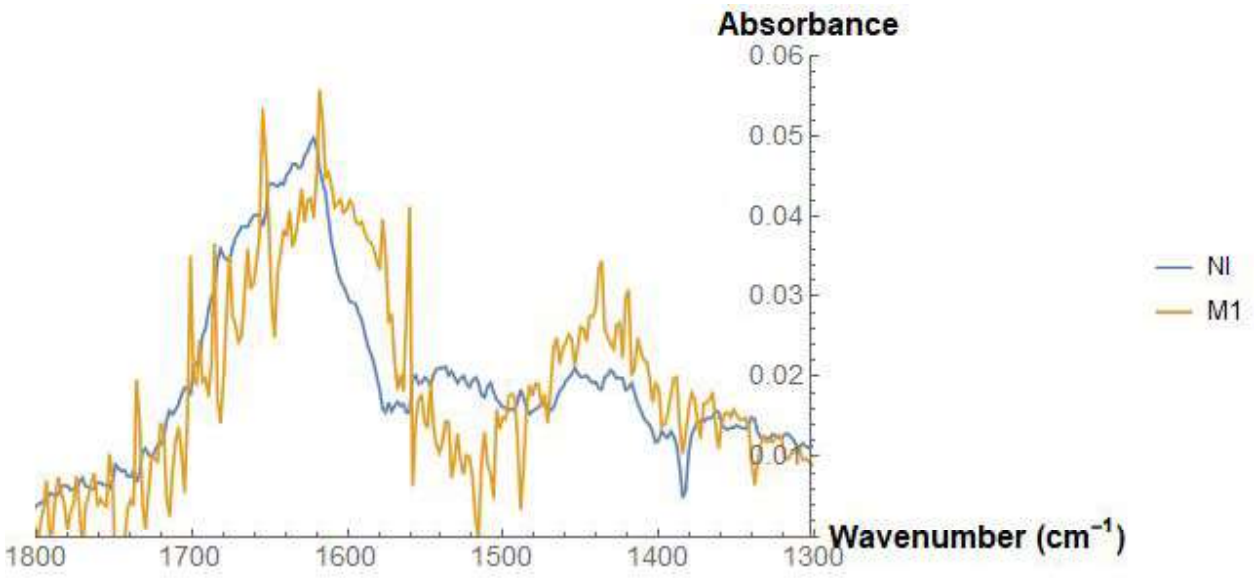

Figure S9: This figures shows the non-averaged spectrum of the M1 and NI sample for the $1800-1300\,\mathrm{cm}^{-1}$ region.

References

Barber, D. (1981). Matrix phyllosilicates and associated minerals in C2M carbonaceous chondrites. *Geochimica et Cosmochimica Acta*, *45*(6), 945–970.

Beck, P., Garenne, A., Quirico, E., Bonal, L., Montes-Hernandez, G., Moynier, F., & Schmitt, B. (2014). Transmission infrared spectra (2–25μm) of carbonaceous chondrites (CI, CM, CV–CK, CR, C2 ungrouped): Mineralogy, water, and asteroidal processes. *Icarus*, *229*, 263–277.

Beck, P., Quirico, E., Montes-Hernandez, G., Bonal, L., Bollard, J., Orthous-Daunay, F.-R., ... others (2010). Hydrous mineralogy of CM and CI chondrites from infrared spectroscopy and their relationship with low albedo asteroids. *Geochimica et Cosmochimica Acta*, *74*(16), 4881–4892.

Botta, O., & Bada, J. L. (2002). Extraterrestrial organic compounds in meteorites. *Surveys in Geophysics*, *23*(5), 411–467.

Bottke, W., Marchi, S., Vokrouhlicky, D., Robbins, S., Hynek, B., & Morbidelli, A. (2015). New insights into the martian late heavy bombardment. In *Lunar and planetary science conference* (Vol. 46, p. 1484).

Bottke, W. F., & Norman, M. D. (2017). The late heavy bombardment. *Annual Review of Earth and Planetary Sciences*, *45*(1).

Bottke, W. F., Vokrouhlickỳ, D., Minton, D., Nesvornỳ, D., Morbidelli, A., Brasser, R., ... Levison, H. F. (2012). An archaean heavy bombardment from a destabilized extension of the asteroid belt. *Nature*, *485*(7396), 78.

Bradley, M. (n.d.). *FTIR Sampling Techniques - Diffuse Reflectance - Sample Preparation.* Retrieved 2017-06-30, from `https://www.thermofisher.com/nl/en/home/industrial/spectroscopy-elemental-isotope-analysis/spectroscopy-elemental-isotope-analysis-learning-center/molecular-spectroscopy-information/ftir-information/ftir-sample-handling-techniques/ftir-sample-handling-techniques-diffuse-reflectance-drifts.html`

Callahan, M. P., Smith, K. E., Cleaves, H. J., Ruzicka, J., Stern, J. C., Glavin, D. P., ... Dworkin, J. P. (2011). Carbonaceous meteorites contain a wide range of extraterrestrial nucleobases. *Proceedings of the National Academy of Sciences*, *108*(34), 13995–13998.

Carr, M. H. (1987). Water on mars. *Nature*, *326*(6108), 30–35.

Chrysostomou, K. (2014). *Methane release from meteoritic material under Mars-like UV radiation.*

Chukanov, N. V. (2013). *Infrared spectra of mineral species: extended library*. Springer Science & Business Media.

Chyba, C., & Sagan, C. (1992). Endogenous production, exogenous delivery and impact-shock

synthesis of organic molecules: an inventory for the origins of life. *Nature*, *355*(6356), 125.
Cleland, C. E. (2002). Methodological and epistemic differences between historical science and experimental science. *Philosophy of Science*, *69*(3), 447–451.
Collins, L. J., Kurland, C. G., Biggs, P., & Penny, D. (2009). The modern rnp world of eukaryotes. *Journal of heredity*, *100*(5), 597–604.
Cronin, J. R., & Pizzarello, S. (1990). Aliphatic hydrocarbons of the murchison meteorite. *Geochimica et Cosmochimica Acta*, *54*(10), 2859–2868.
Dodd, M. S., Papineau, D., Grenne, T., Slack, J. F., Rittner, M., Pirajno, F., ... Little, C. T. (2017). Evidence for early life in earth's oldest hydrothermal vent precipitates. *Nature*, *543*(7643), 60–64.
Engel, M. H., & Macko, S. (1997). Isotopic evidence for extraterrestrial non-racemic amino acids in the murchison meteorite. *Nature*, *389*(6648), 265–268.
Engel, M. H., & Nagy, B. (1982). Distribution and enantiomeric composition of amino acids in the murchison meteorite. *Nature*, *296*(5860), 837–840.
Flynn, G. J. (1996). The delivery of organic matter from asteroids and comets to the early surface of mars. *Earth, Moon, and Planets*, *72*(1-3), 469–474.
Fuchs, G. (2011). Alternative pathways of carbon dioxide fixation: insights into the early evolution of life? *Annual review of microbiology*, *65*, 631–658.
Gomes, R., Levison, H. F., Tsiganis, K., & Morbidelli, A. (2005). Origin of the cataclysmic late heavy bombardment period of the terrestrial planets. *Nature*, *435*(7041), 466.
Hardinger, S. A. (n.d.). *Rna.* Retrieved from `http://web.chem.ucla.edu/~harding/IGOC/R/rna.html`
Hintze, P. E., Buhler, C. R., Schuerger, A. C., Calle, L. M., & Calle, C. I. (2010). Alteration of five organic compounds by glow discharge plasma and uv light under simulated mars conditions. *Icarus*, *208*(2), 749–757.
Hiroi, T., Pieters, C. M., Zolensky, M. E., & Lipschutz, M. E. (1993). Evidence of thermal metamorphism on the c, g, b, and f asteroids. *Science*, *261*(5124), 1016–1018.
Kelley, D. S., Baross, J. A., & Delaney, J. R. (2002). Volcanoes, fluids, and life at mid-ocean ridge spreading centers. *Annual Review of Earth and Planetary Sciences*, *30*(1), 385–491.
Kvenvolden, K., Lawless, J., Pering, K., Peterson, E., Flores, J., Ponnamperuma, C., ... Moore, C. (1970). Evidence for extraterrestrial amino-acids and hydrocarbons in the murchison meteorite. *Nature*, *228*(5275), 923–926.
Kwok, S. (2011). Synthesis of organic matter by stars and its effect on the origin of life on earth. In *Asp conference series.*
Lawless, J. G. (1973). Amino acids in the murchison meteorite. *Geochimica et Cosmochimica Acta*, *37*(9), 2207–2212.
Levison, H. F., Dones, L., Chapman, C. R., Stern, S. A., Duncan, M. J., & Zahnle, K. (2001). Could the lunar "late heavy bombardment" have been triggered by the formation of uranus and neptune? *Icarus*, *151*(2), 286–306.
Mahaffy, P. R., Webster, C. R., Cabane, M., Conrad, P. G., Coll, P., Atreya, S. K., ... others (2012). The sample analysis at mars investigation and instrument suite. *Space Science Reviews*, *170*(1-4), 401–478.
Martin, S. F., & Gilbert, J. C. (2011). *Organic chemistry lab experiments: Miniscale and microscale*. Brooks/Cole.
Martin, W., Baross, J., Kelley, D., & Russell, M. J. (2008). Hydrothermal vents and the origin of

life. *Nature Reviews Microbiology*, *6*(11), 805–814.

Martin, W. F., Sousa, F. L., & Lane, N. (2014). Energy at life's origin. *Science*, *344*(6188), 1092–1093.

McCollom, T. M. (2013). Miller-urey and beyond: what have we learned about prebiotic organic synthesis reactions in the past 60 years? *Annual Review of Earth and Planetary Sciences*, *41*, 207–229.

Millan, M., Szopa, C., Buch, A., Belmahdi, I., Glavin, D. P., Freissinet, C., ... Mahaffy, P. (2017). Influence of oxychlorine phases during the pyrolysis of organic molecules: Implications for the quest of organics on mars with the sam experiment onboard the curiosity rover. *Lunar and Planetary Science*.

Moores, J. E., & Schuerger, A. C. (2012). Uv degradation of accreted organics on mars: Idp longevity, surface reservoir of organics, and relevance to the detection of methane in the atmosphere. *Journal of Geophysical Research: Planets*, *117*(E8).

Neveu, M., Kim, H.-J., & Benner, S. A. (2013). The "strong" rna world hypothesis: Fifty years old. *Astrobiology*, *13*(4), 391–403.

Noller, H., Hoffarth, V., & Zimniak, L. (1992). Unusual resistance of peptidyl transferase to protein extraction procedures. *Science*, *256*, 1416–1419.

O'Leary, M. H. (1981). Carbon isotope fractionation in plants. *Phytochemistry*, *20*(4), 553–567.

Park, R., & Epstein, S. (1960). Carbon isotope fractionation during photosynthesis. *Geochimica et Cosmochimica Acta*, *21*(1-2), 110–126.

Pizzarello, S. (2006). The chemistry of life's origin: a carbonaceous meteorite perspective. *Accounts of Chemical Research*, *39*(4), 231–237.

Pizzarello, S. (2015). Looking for the origin of life in cosmochemistry: Asteroids and their carbon-rich meteorites. *Mètode Science Studies Journal-Annual Review*(6).

Pizzarello, S., & Cronin, J. (2000). Non-racemic amino acids in the murray and murchison meteorites. *Geochimica et Cosmochimica Acta*, *64*(2), 329–338.

Pizzarello, S., & Shock, E. (2010). The organic composition of carbonaceous meteorites: the evolutionary story ahead of biochemistry. *Cold Spring Harbor perspectives in biology*, *2*(3), a002105.

Poch, O., Kaci, S., Stalport, F., Szopa, C., & Coll, P. (2014). Laboratory insights into the chemical and kinetic evolution of several organic molecules under simulated mars surface uv radiation conditions. *Icarus*, *242*, 50–63.

Poch, O., Noblet, A., Stalport, F., Correia, J.-J., Grand, N., Szopa, C., & Coll, P. (2013). Chemical evolution of organic molecules under mars-like uv radiation conditions simulated in the laboratory with the "mars organic molecule irradiation and evolution"(momie) setup. *Planetary and Space Science*, *85*, 188–197.

Rastogi, S. (2005). *Cell biology*. New Age International.

Remusat, L. (2014). Organic material in meteorites and the link to the origin of life. In *Bio web of conferences* (Vol. 2, p. 03001).

Schopf, J. W., Kudryavtsev, A. B., Czaja, A. D., & Tripathi, A. B. (2007). Evidence of archean life: stromatolites and microfossils. *Precambrian Research*, *158*(3), 141–155.

Sephton, M. (2013). Organic Geochemistry of Meteorites-12.1.

Sephton, M. (2014). *Organic geochemistry of meteorites-12.1*. Elsevier Ltd.

Sojo, V., Herschy, B., Whicher, A., Camprubí, E., & Lane, N. (2016). The origin of life in alkaline hydrothermal vents. *Astrobiology*, *16*(2), 181–197.

Sojo, V., Pomiankowski, A., & Lane, N. (2014). A bioenergetic basis for membrane divergence in archaea and bacteria. *PLoS biology*, *12*(8), e1001926.

Stoker, C. R., & Bullock, M. A. (1997). Organic degradation under simulated martian conditions. *Journal of Geophysical Research: Planets*, *102*(E5), 10881–10888.

ten Kate, I. L. (2010). Organics on mars? *Astrobiology*, *10*(6), 589–603.

Varnes, E., Jakosky, B., & McCollom, T. (2003). Biological potential of martian hydrothermal systems. *Astrobiology*, *3*(2), 407–414.

Wetherill, G. (1975). Late heavy bombardment of the moon and terrestrial planets. In *Lunar and planetary science conference proceedings* (Vol. 6, pp. 1539–1561).

Whipple, F. L. (1966). Chondrules: suggestion concerning the origin. *Science*, *153*(3731), 54–56.

Zhang, B., & Cech, T. R. (1997). Peptide bond formation by in vitro selected ribozymes. *Nature*, *390*(6655), 96–100.